Electronic Supplementary Material (ESI) for Physical Chemistry Chemical Physics.

Supplementary Information: The Interaction of Size-Selected Ru_3 Clusters with Sputter-Deposited TiO_2: Depth-Profiling of Encapsulated Clusters

Liam Howard-Fabretto[1,2], Timothy J. Gorey[3], Guangjing Li[3], DJ Osborn[4], Siriluck Tesana[5], Gregory F. Metha[4], Scott L. Anderson[3], and Gunther G. Andersson[1,2]*

1 Flinders Institute for Nanoscale Science and Technology, Flinders University, Adelaide, South Australia 5042, Australia

2 Flinders Microscopy and Microanalysis, College of Science and Engineering, Flinders University, Adelaide, South Australia 5042, Australia

3 Chemistry Department, University of Utah, 315 S. 1400 E., Salt Lake City, UT 84112, United States

4 Department of Chemistry, University of Adelaide, Adelaide, South Australia 5005, Australia

5 The MacDiarmid Institute for Advanced Materials and Nanotechnology, School of Physical and Chemical Sciences, University of Canterbury, Christchurch 8141, New Zealand

*Corresponding author: Gunther G. Andersson

Email: gunther.andersson@flinders.edu.au.

Address: Physical Sciences Building (2111) GPO Box 2100, Adelaide 5001, South Australia

Experimental

TiO_2(110) Preparation

The sample preparation for TiO_2(110) followed the method used in recent publications by Anderson *et al.* [1,2]. The TiO_2(110) was initially treated by heating to 1050 K for 1 hour under ultra-high vacuum (UHV). This has been shown to induce oxygen defects in the bulk of TiO_2(110), which turns the sample blue and induces conductivity [3-5]. This allows XPS to be performed without suffering sample charging and Fallows charged Ru_3^+ clusters to be neutralised when deposited by the CS. Additionally, before each experiment the sample was sputtered with 3 keV Ar^+ for 20 minutes, then heated to 900 K for 20 minutes. Prior to cluster depositions, 6 x 10^{14} Ar^+ ions/cm^2 was sputtered onto the TiO_2(110).

Chemical Vapor Deposition (CVD)

Chemical vapor depositions (CVD) are performed using the UHV loading chamber of the Flinders University UHV apparatus, except for the ARXPS sample measured at the Australian Synchrotron which will be described separately below. Due to their high vapor pressures, metal carbonyl clusters only typically require vacuum in the range of 10^{-7} mbar to vaporise at room temperature [6]. From in-house deposition testing, pressures of approximately 4 x 10^{-6} mbar or lower are deemed suitable for depositions to proceed at a fast enough rate at room temperature. For each deposition, a sample vial was loaded with 2.13 mg ± 0.05 mg of $Ru_3(CO)_{12}$. 2 mL of dichloromethane was then added to the vial which was ultrasonicated for 1 minute to dissolve the clusters. The outside of the vial was then cleaned with ethanol. The dichloromethane was left to evaporate for ~30 minutes in a fume hood leaving a film of ligated clusters coated on the inside wall of the vial. This vial was then loaded into the vacuum chamber on a manipulator arm which could be retracted behind a sheath. For deposition the vial was moved underneath the sample and the $Ru_3(CO)_{12}$ were allowed to evaporate/deposit onto samples, coating the entire sample area. Deposition times were 120 minutes for RF-TiO_2 and 30 minutes for TiO_2(110). For the ARXPS CVD-$Ru_3(CO)_{12}$/HDS-RF-TiO_2 sample, the CVD was performed *in situ* at the Australian Synchrotron in a separate loading chamber. The deposition vial could not be brought as close to the sample, so the $Ru_3(CO)_{12}$ vial was heated to 313 K to increase the deposition rate and clusters were deposited for 90 minutes.

Cluster Source Deposition

Ru_3 were produced in a cluster source (CS) under UHV by pulsed laser vaporisation (LaVa) of a 99.9% pure Ru target. Vaporised target atoms were pulsed into a helium gas flow, immediately followed by supersonic expansion of the metal atoms into the vacuum. A RF quadrupole ion guide was set to collect only positively charged clusters, and the cluster beam was angled by 20° to remove neutral clusters. A quadrupole mass filter filtered for a specific mass/charge ratio. As most clusters are singly charged [7,8] this can be treated as a cluster mass selection process. The clusters then passed through a 2 mm aperture into the main UHV chamber where they were deposited onto a closely positioned substrate to achieve 2 mm diameter cluster spots.

For each CS-deposition, the substrates were liquid N_2 cooled to 180 K, followed by a quick temperature flash to 700 K to remove any adventitious hydrocarbons. The cluster depositions were initiated at 300 K, and continued as the sample cooled to 180 K. The neutralisation current was measured and summed during depositions to ensure the amount of deposited cluster material was consistent. Each CS-deposition deposited nominally 1.5 x 10^{14} atoms/cm^2 (0.5 x 10^{14} clusters/cm^2). A 1 eV/atom positive retarding potential was applied to the substrates during depositions to reduce the impact energy of the clusters; this is critical in preventing cluster fragmentation on impact [9]. Previous studies of the deposition of small Ir clusters onto TiO_2 and SiO_2 showed that impact energies in the tens of eV/atom are required to embed the clusters into these substrates (*e.g.* at least 10 eV/atom for small Ir clusters on TiO_2) [10,11]. Thus, the 1 eV/atom deposition energy is considered suitable to not cause cluster damage or embedding during depositions of Ru clusters.

List of Samples

Separate samples were prepared for each measurement, to ensure that sample damage is minimised prior to analysis. Table S1 shows a list of all analysed samples, and whether they were measured *in situ* or *ex situ*.

Table S1: List of samples prepared and analysed.

Sample Number	Cluster Type	Substrate Type	Analytical Techniques	*In situ* or *ex situ*
1	CVD-$Ru_3(CO)_{12}$	HDS-RF-TiO_2	TD-XPS	*In situ*
2	CVD-$Ru_3(CO)_{12}$	TiO_2(110)	TD-XPS	*In situ*
3	CS-Ru_3	NS-RF-TiO_2	TD-XPS	*In situ*
4	CS-Ru_3	SiO_2	TD-XPS	*In situ*
5	CVD-$Ru_3(CO)_{12}$	HDS-RF-TiO_2	ARXPS	*In situ*
6	CS-Ru_3	HDS-RF-TiO_2	ARXPS	*Ex situ*
7	CVD-$Ru_3(CO)_{12}$	HDS-RF-TiO_2	TD-LEIS	*In situ*
8	CS-Ru_3	SiO_2	TD-LEIS, Series LEIS	*In situ*
9	CS-Ru_3	NS-RF-TiO_2	TD-LEIS	*In situ*
10	CS-Ru_3	LDS-RF-TiO_2	TD-LEIS	*In situ*
11	CS-Ru_3	HDS-RF-TiO_2	TD-LEIS	*In situ*
12	CVD-$Ru_3(CO)_{12}$	HDS-RF-TiO_2	STEM	*Ex situ*

TD-XPS
Instrumentation

At Flinders University, a non-monochromatic X-ray source with an Mg anode was used with a Phoibos 100 hemispherical analyser (SPECS, Germany). At The University of Utah, a non-monochromatic X-ray source with an Al anode was used (Physical Electronics); this featured an area-selective lens allowing the 2 mm CS cluster spots to be probed with minimal effects from the surrounding substrate. For both instruments 10 eV pass energies were used, and the photons had an incidence angle of 54.7° to the surface and ejected electrons were measured orthogonal to the surface.

Peak Fitting

CasaXPS was used to fit the peaks in XPS spectra. Shirley backgrounds [12] were subtracted from each measured spectrum when integrating the fitted peaks. Individual component peaks are added to the XPS spectra using CasaXPS and typically fitted using the symmetrical Gaussian-Lorentzian GL(30) line shape. As a constraint each of these must be justified with a physical meaning.

Every XPS spectrum featured C 1s peaks to some extent, and two peaks were always present; these were due to C-C or C-H bonding at 285.0 eV, and C=O or C-O-C bonding at 287.0 eV. A third carbon peak likely due to O=C-O bonding at 289.4 eV was sometimes present but was most often removed by UHV heat treatment and/or sputtering. These results were comparable to previously reported assignments for carbon contamination on SiO_2 substrates [13].

Care was paid when fitting the Ru 3d doublet for clusters, because the 285.0 eV adventitious C 1s peak overlapped with the Ru 3d doublet. To aid with fitting the Ru $3d_{3/2}$ peak, an Ru reference metal was analysed with XPS and used as a fitting model for cluster spectra. This spectrum is shown in the supplementary information of our previous study [14], and the determined line shape is shown in Table S2. When comparing the $3d_{5/2}$ to $3d_{3/2}$ peaks for the Ru reference sample, the peak separation was 4.17 eV, peak area ratio was 3:2, and FWHM ratio was 1:1.15. For Ru cluster XPS peak fitting, these values were used to lock the size and shape of the $3d_{3/2}$ peak to the $3d_{5/2}$ peak.

Ru 3d peaks were fitted with asymmetrical line shapes, which is typical for transition metal 3d peaks. Work has been done by Morgan [15] investigating the best way to fit this asymmetry for Ru in different chemical environments. The extent of the peak asymmetry is dependent on the chemical nature of Ru, and the measured asymmetry may also be effected by the resolution of the XPS instrumentation [15-17]. A modified version of the line shape used by Morgan for metallic Ru was used to fit the Ru reference sample XPS data. The LF line shape used corresponds to a “Lorentzian asymmetric line shape with tail damping” in CasaXPS. To the best of the author’s knowledge, there are no published asymmetry results for Ru in cluster form, and thus the line shapes published by Morgan were used as a starting point and were altered to best fit the line shape seen for the Ru clusters on each instrument (see Table S2). A special case was made for the as-deposited ligated Ru clusters; these were fitted with symmetrical GL(30) line shapes due to the ligands.

Table S2:Line shapes used for fitting Ru 3d peaks from XPS in different scenarios.

Measurement	XPS Instrument	Ru $3d_{5/2}$ line shape	Ru $3d_{3/2}$ line shape
Metallic Ru reference sample	Flinders University	LF(0.8,1.3,500,180)	LF(1.15,1.5,500,50)
Ru clusters	Flinders University	LF(0.75,1.25,500,250)	LF(0.8,1,500,250)
Ru clusters	The University of Utah	LF(0.7,1.8,25,280)	LF(0.7,1.8,25,280)
Ru Clusters	Australian Synchrotron	LF(1.2,1.8,500,250)	LF(1,1.8,500,250)
As-deposited, Ligated Ru clusters	All	GL(30)	GL(30)

Atomic concentrations in percentage (At%) were determined using XPS by fitting all the peaks and integrating them to determine their area, and then calibrating the areas by dividing by the XPS sensitivity factors found in the Handbook of X-ray Photoelectron Spectroscopy [18]. The atomic ratio was determined by dividing the calibrated peak areas for each element by the total calibrated peak area for all elements, and then multiplied by 100% to determine the At%.

The relative resolution for At% varied depending on the size of the peaks, and whether they overlapped with other peaks. Due to this, the relative fitting uncertainty in At% for each peak of interest was estimated by determining the largest range of peak areas which resulted in what was considered to be a reasonable fitting of the measured spectra. The relative uncertainty for At% of Ru 3d cluster peaks was ~4%. For substrate materials, the peaks were much larger due to the higher atomic concentration, so the relative At% uncertainty for Ti^{4+} 2p, O 1s, and Si 2p in SiO_2 and TiO_2 substrates are each ~1%. The Ti^{3+} and Ti^{2+} 2p peaks each have a relative uncertainty of ~24%. The fitting procedure was kept consistent for all Ti 2p spectra to minimise the relative error, and as such it was estimated that the relative uncertainty in the $Ti^{defects}$ At% when comparing between the samples was lower at ~15%.

For $Ti^{defects}/Ti^{Total}$ ratios, the ~15% $Ti^{defects}$ 2p fitting uncertainty was taken to be the dominant uncertainty. When C/Ru ratios are presented, the uncertainty in the fitting of C was negligible compared to Ru, and the relative uncertainty was taken as ~4%. CO/Ru atomic ratios have

a summed uncertainty of ~13%. Due to this fitting uncertainty as well as the CO contaminant baseline subtractions which were necessary, the absolute error in the CO/Ru atomic ratio for supported clusters was estimated to be ± ~0.5.

Surface Coverage Estimation

The surface coverage of cluster material was estimated for each cluster deposition where XPS was performed. The surface coverages are presented in units of % ML, which is the percentage relative to an entire monolayer (ML) of coverage. This calculation solved for the surface concentration required to achieve the measured XPS At% for Ru. For this estimation the clusters were assumed to be present in only a single ML on the surface with negligible stacking of atoms and no mixing of cluster and substrate layers. The Ru-Ru bulk interatomic distance was taken as 0.265 nm [19], which was used as the layer thickness for deposited Ru clusters. The contribution of individual atoms to the XPS spectra are reduced as the depth of the atom into the surface increases, which was factored into the calculation using the IMFP of electrons in TiO_2. An IMFP of 1.8 nm was used based on a study which calculated the IMFP of electrons in thermally grown TiO_2 based on experimental measurements at an excitation energy of 1250 eV [20].

A range of factors contribute to the uncertainty in surface coverage estimations. These include errors in the calculated XPS At% for the clusters, differences between atomic sensitivity factors in our detector setup and in the XPS handbook [18], and any inaccuracy in the IMFP of electrons in the substrate. The absolute error in surface coverage was therefore assumed to be ~100%. However, the relative error comparing between samples only comes from the cluster At% fitting uncertainty and was ~4%. While the ~100% error can be considered high, the surface coverage estimation was intended to give the scale of the surface coverage of clusters used in the experiments, and for relative comparisons between samples the results were deemed reliable.

ARXPS

Synchrotron X-ray Source

ARXPS measurements were performed at the Australian Synchrotron soft X-ray beamline. ARXPS allows a concentration depth profile of the sample to be determined by changing the observation angle of the emitted photoelectrons. XPS measurements were taken at observation angles of 0˚, 30˚, 45˚, 55˚, and 60˚, which are suitable angels to avoid severe effects related to the elastic scattering of photoelectrons [101]. To determine a depth profile from an ARXPS measurement, a model was made and fitted to the experimental data for

measured concentrations at each observation angle. Two samples were analysed; CVD-$Ru_3(CO)_{12}$/HDS-RF-TiO_2 deposited *in situ*, and CS-Ru_3/HDS-RF-TiO_2 deposited *ex situ* at the University of Utah. Each individual ARXPS measurement was performed at 5 temperatures between room temperature and 723 K for each sample.

The synchrotron X-ray excitation energy used was 720 eV, and the beamline is equipped with a Phoibos 150 HSA at 10 eV pass energy (SPECS, Germany). The synchrotron beam entrance slit was set to 20 μm. The beam size at the sample was ~0.1 mm^2. The total beam intensity at the sample was measured using a GaAs detector, where the energy per GaAs electron-hole pair energy was taken as 4.18eV [21]. Assuming the entirety of each 720 eV photon was transferred into electron-hole pairs, the beam flux was 7 x 10^{14} photons/cm^2/s.

For the CVD-$Ru_3(CO)_{12}$/HDS-RF-TiO_2 sample, it was noticed that synchrotron X-rays partially remove the CO ligands from $Ru_3(CO)_{12}$ clusters, which was investigated by a series of XPS measurements shown in the supplementary information (pages 22-23). To avoid beam effects for the main ARXPS measurements, the CVD-$Ru_3(CO)_{12}$/HDS-RF-TiO_2 sample was scanned in a grid such that each angle and temperature measurement was on a fresh area of the sample.

Peak Fitting

In general, the same XPS data analysis procedures described for TD-XPS were used for ARXPS. Differences from the standard procedure are noted here. To determine the atomic sensitivity factors of interest at a 720 eV excitation energy, a sample was scanned at both 720 eV and 1253.6 eV (the Mg Kα excitation energy) to find the ratios of peak areas between the results. When determining the Ru At%, C 1s peaks were ignored in the calculations to minimise effects of hydrocarbon contamination on the results. The increased resolution and count rate of the Australian Synchrotron XPS instrument improved the fitting uncertainties compared to the laboratory-based measurements; Ru At% was ± 2%, CO At% was ± 2%, and CO/Ru atomic ratio was ± 4%. The absolute error for CO/Ru atomic ratio was estimated to be higher at ~10%. The accuracy for Ru 3d peak locations was ± 0.05 eV when comparing between measurements of the same sample performed in series, or ± 0.1 eV comparing different samples.

ARXPS Model Calculation

A similar evaluation algorithm was used in determining concentration depth profiles as used by Eschen *et al.* [22], and more recently Andersson *et al.* [23]. In this procedure the measured Ru At% at each angle was fitted to a model, using the concentration of Ru at

various sample depths as a fitting parameter. The difference between the measured and modelled At% at each angle was minimised to determine the concentration depth profile. The Excel solver function was used to minimise the differences. The ratio of $\frac{|measured\ At\% - modelled\ At\%|}{measured\ At\%}$, was used as a measure for the difference between the experimental and results for Ru At%. For the ARXPS depth profiles, the values of layer concentration (%) in each depth layer were estimated to have an uncertainty of ± 20%. The resolution in Ru penetration depth for ARXPS was ± 0.3 eV, based on half the defined layer width used in the calculations.

The following assumptions were used in the modelling process: a) The observation depth varied with the cosine of the emission angle, θ. b) Once beyond a finite depth from the surface into the bulk, the sample has a consistent, homogeneous composition. c) Possible variations in sample density which effected the composition are neglected. d) The inelastic mean free path (IMFP) was constant from the bulk to the surface. e) the distance from the surface into the depth of the sample was modelled as a number of finite layers, each having a homogenous composition. The mean free path of electrons in the sample material depends on the composition of the sample and will influence the distance photoelectrons can travel through the sample, which was factored into the calculation and taken as 1.2 nm for 720 eV photons [20].

LEIS

Technique

In situ LEIS measurements were performed on samples at both Flinders University and the University of Utah using same settings. 1 keV He^+ ions were produced using ion guns, which were incident on the sample at 45°, and backscattered He^+ was at a scattering angle of 135°. The backscattered He^+ ions were detected with the same HSA detectors which were used on each UHV apparatus for XPS (see above). To minimize damage from He^+ projectile impacts, scan times were kept as low as possible to achieve reasonable resolution, and the He^+ beam was on only during scans. Preliminary testing performed prior to the main TD-LEIS measurements is shown in the supplementary information, pages 25-26.

Surface Sensitivity

LEIS is mostly sensitive to the elemental composition of the outermost layer due to the higher neutralisation probability for He^+ projectiles backscattered from layers below the outermost layer [24]. This is due to a combination of shadowing (upper atoms shielding lower atoms from He^+), blocking (backscattered He^+ being shielded due to sample geometry), and

the reduced ion survival probability due to the increased time of interaction between the projectile and sample. There is, however, a finite probability for backscattering of He^+ projectiles from deeper layers [25].

Reproducibility

To test the reproducibility of the spectra for the LEIS at Flinders University, RF-TiO_2 was scanned 20 times throughout one day and no differences in the results were found. Conversely, the high reproducibility of results from the University of Utah LEIS was well known prior to this study this had been specifically tested [26], and the system had been used in numerous studies after this [1,2,24,27-32].

Data Analysis

The surface peaks in measured LEIS spectra were integrated to determine cluster/substrate peak area ratios for the LEIS samples. The cluster/substrate peak area ratio was used as a measure of the concentration of Ru accessible to LEIS. The uncertainty in Ru peak area ratios was estimated as ± 8%. The stopping power of titania was calculated using the software package SRIM [33] for 1.10 keV He^+ in TiO_2 to be 30 eV/nm ± 3 eV/nm. Calculations were performed using Bragg's rule [34]. Ion doses were estimated for each sample using the neutralisation current at the sample and scan times. The neutralisation current was a suitable measurement for the number of incoming clusters because >99% of incoming He^+ ions are neutralised [25,35].

Estimating Cluster Damage

For each sample measured with LEIS the total cumulative cluster removal caused by the He^+ beam was estimated in terms of Ru MLs, using the percentage of Ru which was removed from the surface. To determine this, it was assumed all Ru was on the topmost layer, and that the LEIS signal was directly proportional to the Ru surface coverage. The removal rate of Ru from an SiO_2 surface, R, was determined experimentally to be R = -1.2 x 10^{-2} atoms/ion (see supplementary informations page 26). The packing density of a Ru ML, D, was estimated. Ru unit cells are close packed hexagonal, and if the top is sliced off the unit cell (to make a surface layer) the length of a hexagonal side is 0.27 nm [36], with a unit cell face area of 1.89 x 10^{-15} cm^2. The face features two atoms, and thus the estimated packing density, D, of an Ru ML was ~9.47 x 10^{-16} cm^2/atom.

The estimated cluster removal for each sample was determined using the same method, and here an example calculation is provided for the CVD-$Ru_3(CO)_{12}$/HDS-RF-TiO_2 sample; the cumulative Ru dose per area for this measurement was 5.95 x 10^{15} ions/cm^2. The ion

dose per area was multiplied by R to determine the number of Ru atoms being removed per area; 7.14 x 10^{13} atoms/cm^2 (this assumed a full ML of Ru was present).This was then found in terms of MLs of Ru removed, by multiplying by D. In this case ~6.8 x 10^{-2} ML of Ru was removed by the beam, or 6.8% ML.

STEM

A cross-section of a CVD-$Ru_3(CO)_{12}$/HDS-RF-TiO_2 sample was analysed using high resolution scanning transmission electron microscopy (STEM). For this process, a sample was prepared under UHV by performing CVD and then heating to 723 K, before being transferred *ex situ* to another UHV system. Here, a protective layer was added to the surface by evaporative deposition of 50-100 nm of carbon followed by sputter deposition of 10-20 nm of platinum. A cross section was then cut using a 30 kV focussed ion beam (FIB) of Ga^+ and separated from the main body of the sample. This was transferred *ex situ* to the STEM instrument (FEI Titan Themis 80-200) for analysis, which was done side-on to image the depth into the surface. Energy-dispersive X-ray spectroscopy (EDX) was used alongside STEM to generate an atomically-sensitive image.

Results

TD-XPS

Sample Summary

Table S3 displays the Ru At% and Ru surface coverage determined for each TD-XPS sample, as well as details about the TD-XPS measurements.

Table S3: Summary of Ru At% and Ru $3d_{5/2}$ BE for each TD-XPS sample. At% and surface coverages are averaged from all temperatures for each sample. The temperature ranges for TD-XPS of each sample are shown. The as-deposited BE is at the deposition temperature, while the heat treated BE is at 723 K for CVD samples, and 800 K for CS samples.

Deposition	Substrate	Ru At% (%)	Ru Surface Coverage (% ML)	TD-XPS Range (K)	As-Deposited BE (eV)	Heat-Treated BE (eV)
CVD-$Ru_3(CO)_{12}$	HDS-RF-TiO_2	1.11	8.0	298 - 873	281.6	280.6
CVD-$Ru_3(CO)_{12}$	TiO_2(110)	2.41	17.2	298 - 873	281.2	280.5
CS-Ru_3	NS-RF-TiO_2	0.44	3.2	190 - 800	280.3	280.5
CS-Ru_3	SiO_2	0.51	3.7	190 - 800	280.7	280.7

The Ru surface coverages in Table S3 show that the coverage ranged from 3.2% ML to 17.2% ML. The pores in the RF-TiO_2 substrates likely explain the reason for the higher surface coverage of CVD-$Ru_3(CO)_{12}$ on TiO_2(110) compared HDS-RF-TiO_2 (see Figure S18 and Figure S21). Since all samples are a small fraction of a ML, any effects related to surface coverage (*i.e.* due to cluster-cluster interactions) are considered negligible.

Ru 3d/C 1s Region

The Ru 3d and C 1s peaks overlap in BE and are fitted together. The TD-XPS results for the $Ru_3(CO)_{12}$ samples are shown in Figure S1. A minimum of 5 temperatures were measured per sample, however for readability the results are only shown at room temperature, 373 K, and 723 K. For all spectra in Figure S1 the lower BE features are related to Ru $3d_{5/2}$ and the higher BE features are related to the overlap of Ru $3d_{3/2}$ and C 1s. For each sample, heating to 373 K and 723 K sequentially reduced the BE of the Ru 3d feature. Examples of the peak fitted XPS spectra for $Ru_3(CO)_{12}$-deposited TD-XPS samples are shown in Figure S2. The CVD-$Ru_3(CO)_{12}$/HDS-RF-TiO_2 sample is used as an example, but CVD-deposited samples are fit using the same procedure.

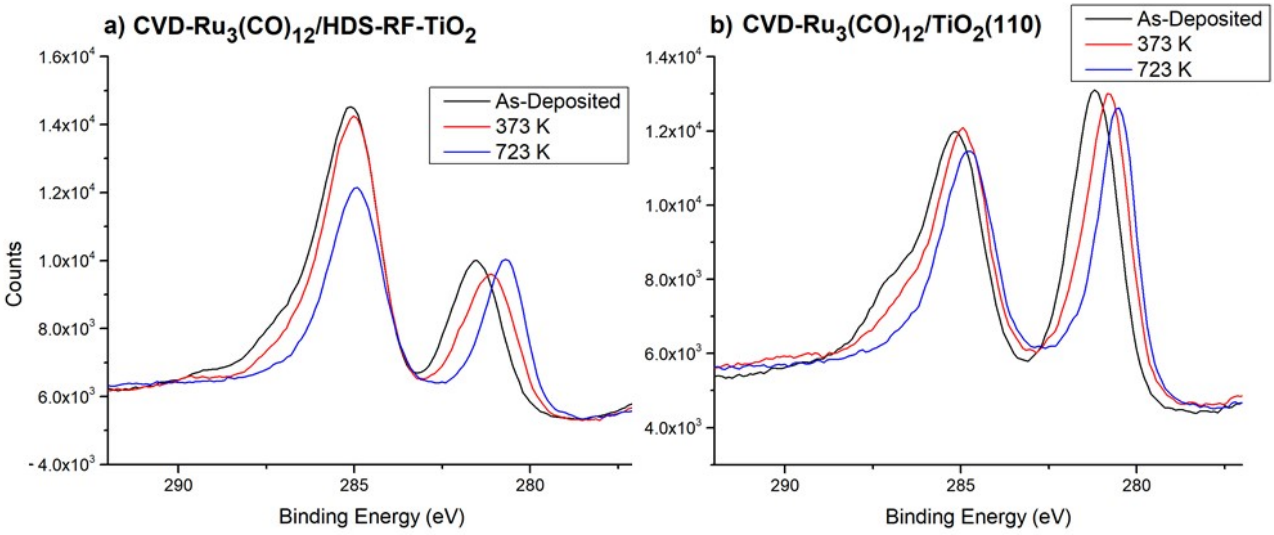

Figure S1: TD-XPS spectra of the Ru 3d/C 1s region for $Ru_3(CO)_{12}$ samples as-deposited, at 373 K, and at 723 K. a) CVD-$Ru_3(CO)_{12}$/HDS-RF-TiO_2. b) CVD-$Ru_3(CO)_{12}$/TiO_2(110).

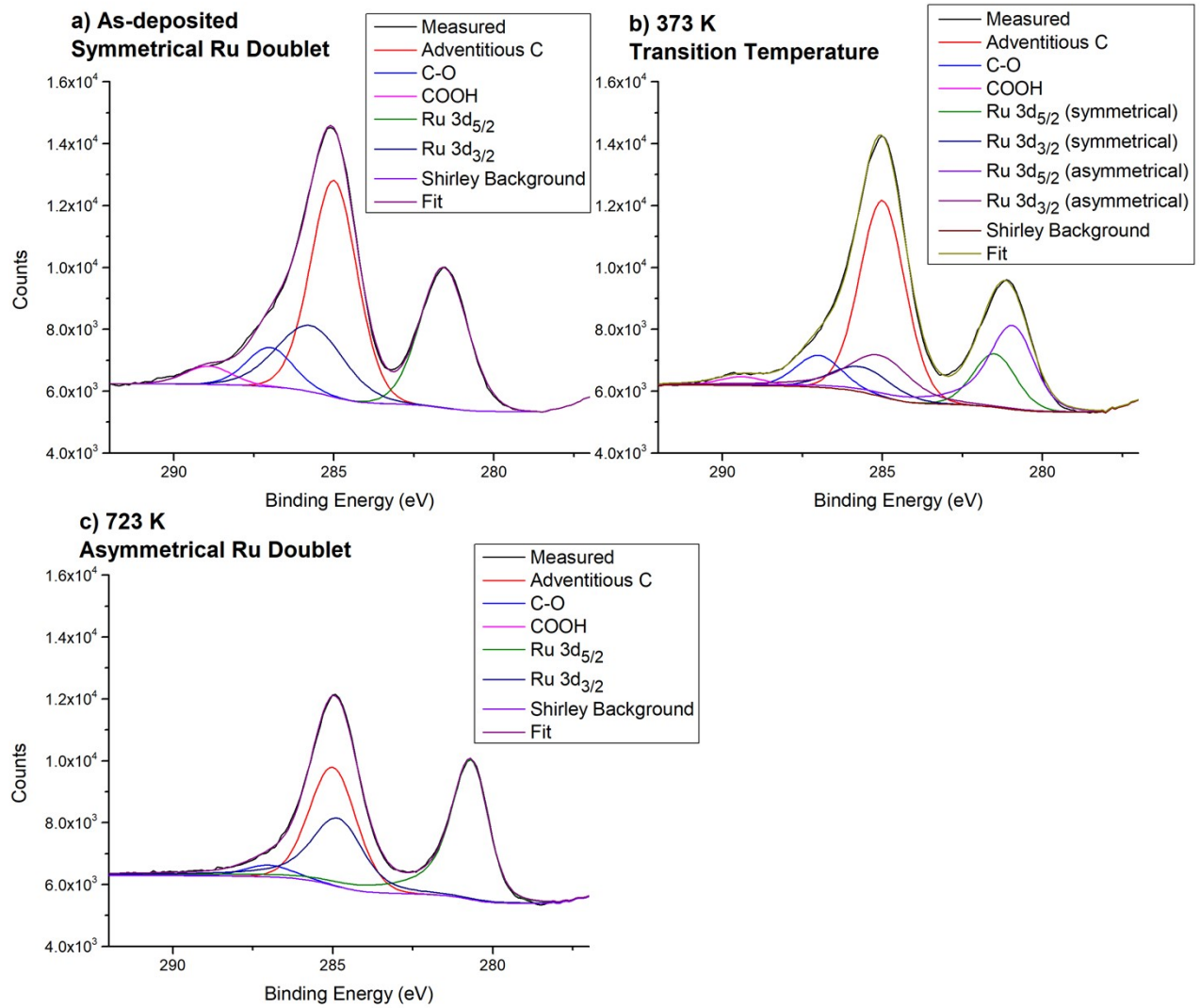

Figure S2: Example fittings of the Ru 3d/C 1s XPS region for the TD-XPS of CVD-$Ru_3(CO)_{12}$/HDS-RF-TiO_2. a) As-deposited at room temperature. b) Heated to 373 K. c) Heated to 723 K. The fitting procedure is identical for CVD-$Ru_3(CO)_{12}$/TiO_2(110).

Figure S2 shows that the Ru 3d doublet related to the $Ru_3(CO)_{12}$ clusters are fitted with a symmetrical line shape as-deposited (before heating), but the peak changed to an asymmetrical shape by heating to 423 K. At 373 K the Ru is transitioning between states, and both symmetrical and asymmetrical doublets are required for an accurate fitting in the model. An asymmetrical line shape is typical for the Ru 3d peak from bulk, metallic Ru [15]. Due to this, the change of line shape with heating provides evidence for a shift towards more metallic properties for the Ru, associated with the removal of the CO ligands due to heating.

The TD-XPS results for the CS-deposited Ru_3 samples are shown in Figure S3. For readability, the results are only shown at room temperature, 350 K, and 700 K for each sample. There is a slight shift towards higher Ru $3d_{5/2}$ BE due to heating for CS-Ru_3/NS-RF-TiO_2, while there is little change in BE for CS-Ru_3/SiO_2. Examples of the peak fitting for the CS-deposited TD-XPS samples are shown in Figure S4.

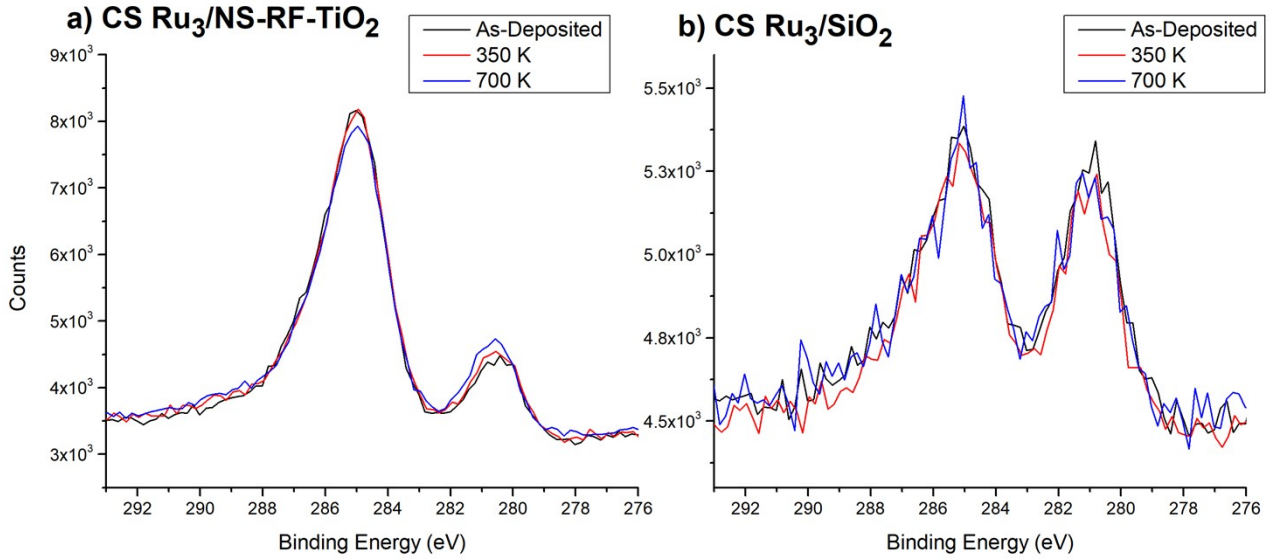

Figure S3: XPS spectra of the Ru 3d/C 1s region for CS-Ru_3 TD-XPS samples, as-deposited, at 350 K, and at 700 K. a) CS-Ru_3/NS-RF-TiO_2. b) CS-Ru_3/SiO_2.

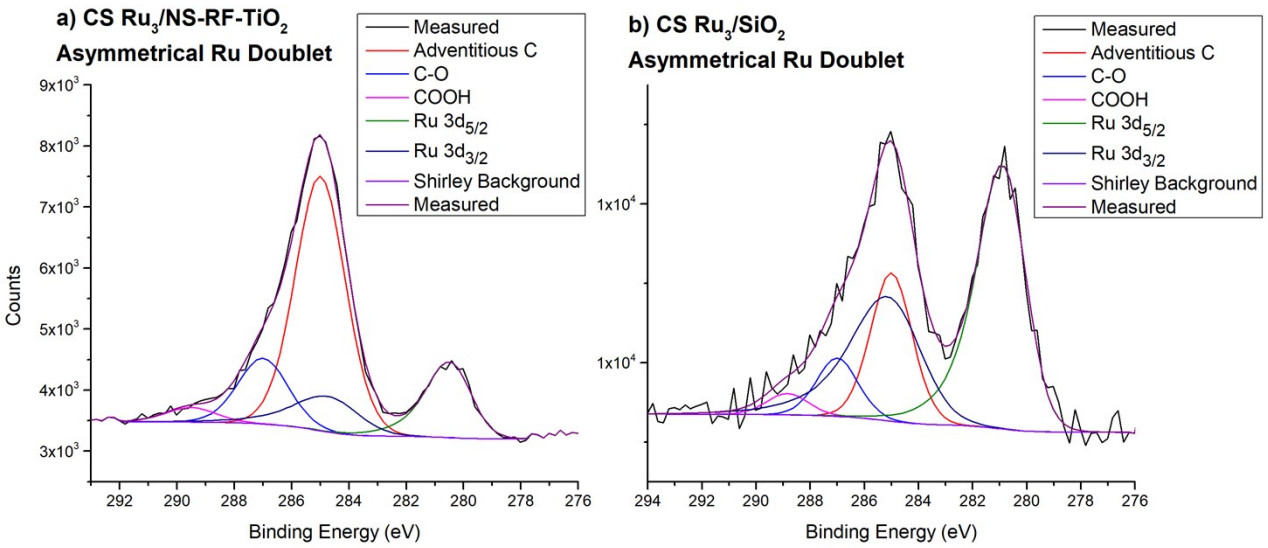

Figure S4: Example fitting of the Ru 3d/C 1s XPS region for CS-Ru_3 TD-XPS samples. a) CS-Ru_3/NS-RF-TiO_2 as deposited. b) CS-Ru_3/SiO_2 as deposited. Asymmetrical Ru doublets are used at all temperatures for both samples.

For CS-Ru_3, the Ru peak shape is asymmetrical at all measured temperatures for both samples. This contrasts with the ligated $Ru_3(CO)_{12}$ samples, where the Ru peak shape is symmetrical at room temperature. This aligns with the interpretation that the presence of CO ligands is influencing the asymmetry of the peaks.

Ti 2p Region

Three examples of fitted spectra are shown for the Ti 2p XPS region in Figure S5. These are given as examples because they represent the three types of TiO_2 substrates used. Peak fitting for all other measurements of the Ti 2p region followed these procedures.

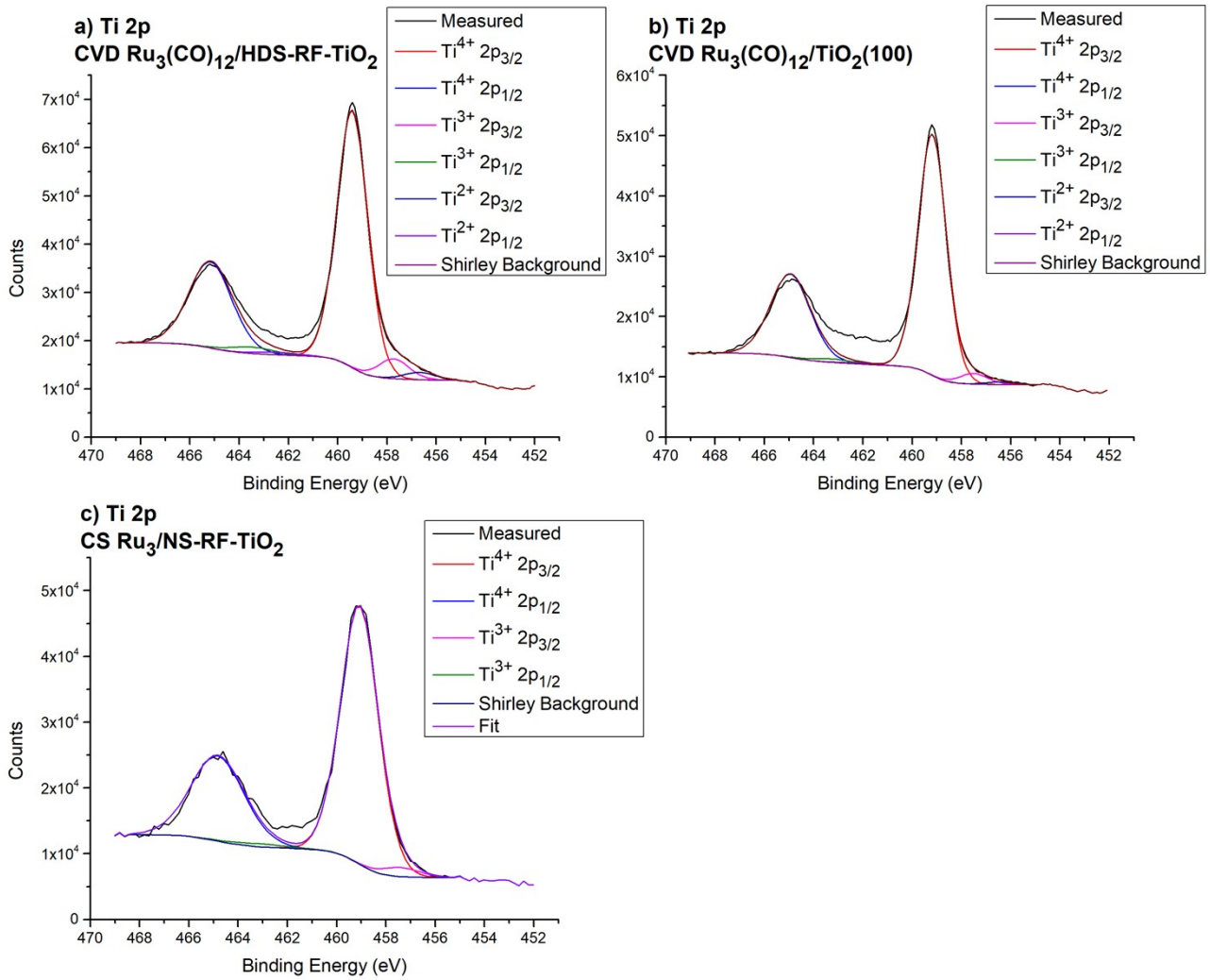

Figure S5: Example Ti 2p XPS region fittings for substrates with as-deposited clusters. a) CVD-$Ru_3(CO)_{12}$/HDS-RF-TiO_2. b) CVD-$Ru_3(CO)_{12}$/TiO_2(110). c) CS-Ru_3/NS-RF-TiO_2. Note there is a consistent under-fit between the Ti doublet peaks due to a changing background signal.

There is a difference in Ti 2p fitting procedures between Figure S5a-b and Figure S5c. This difference is due to the slightly different line shapes for the Flinders University XPS (used for ligated samples) and the University of Utah XPS (used for CS-deposited samples). All TiO_2 samples measured with the Flinders University XPS instrument had some signal present in the location of Ti^{2+} which is not visible at The University of Utah; the Ti^{2+} is most likely not actually present on the surface and is just an artefact of the intrinsic line shape related to the detector. The key difference between the apparatuses is the difference between Mg Kα excitation (Flinders University) and Al Kα excitation (The University of Utah), which is known to effect the line shape [18].

Figure S5 and Figure S5b are fitted similar to one another. Three unique Ti doublets are modelled, corresponding to Ti^{4+}, Ti^{3+}, and Ti^{2+}. The Ti 2p peaks are present at 459.6 eV, 457.9 eV, and 546.8 eV, respectively. For CS-Ru_3 depositions, the Ti 2p fitting procedure is

performed according to Figure S5c; only two doublets are used corresponding to Ti^{4+} and Ti^{3+}. For this study Ti^{3+} and Ti^{2+} are summed and referred to as $Ti^{defects}$. For the purposes of the TD-XPS experiment the Ti 2p fitting differences are considered negligible to the result.

Analysis

The Ru At% TD-XPS results are shown in Figure S6. The Ru At% as measured by XPS is not significantly changing with the temperature.

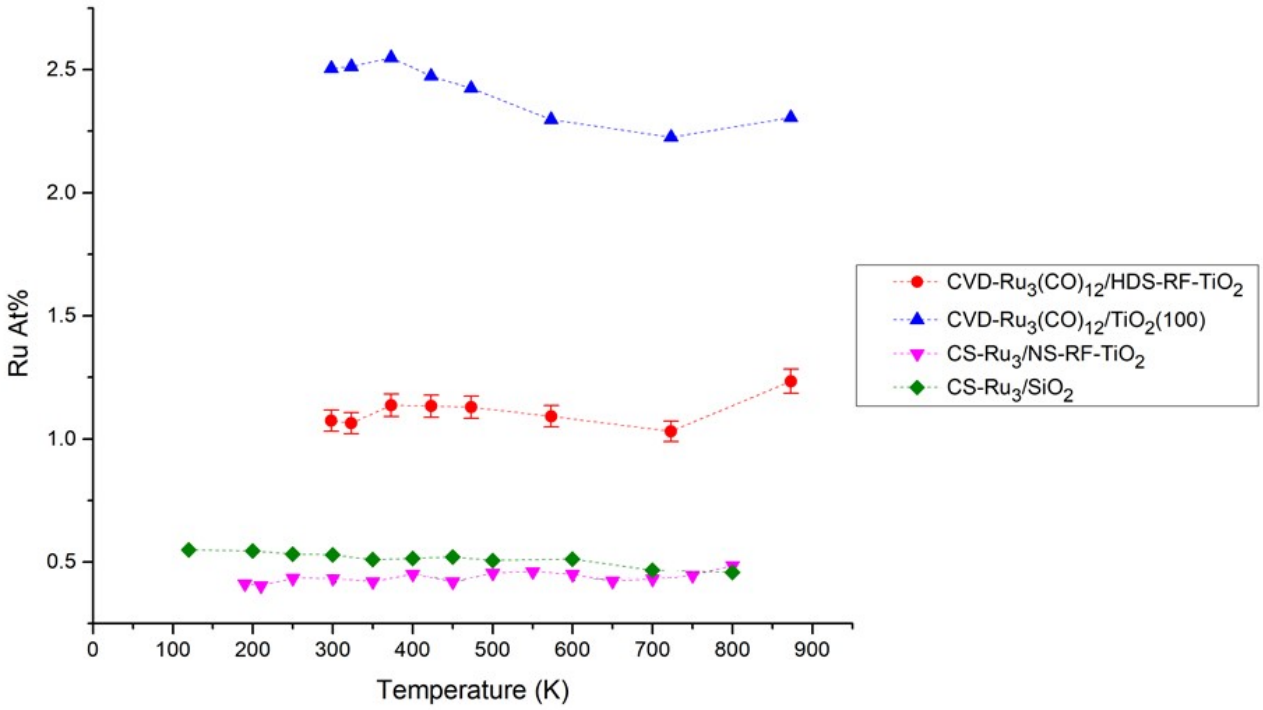

Figure S6: TD-XPS results for Ru At%. The uncertainty in Ru At% is ~4% which is shown in the error bars. Error bars are the same for all samples but are only displayed for one to prevent overlapping.

The Ru $3d_{5/2}$ BEs as function of temperature are shown in Figure S7. When comparing the results from $Ru_3(CO)_{12}$ depositions and CS depositions it has to be noted that heating of $Ru_3(CO)_{12}$ removes the CO ligands [37,38] resulting in a significant decrease in BE. This did not occur for CS-Ru_3 samples.

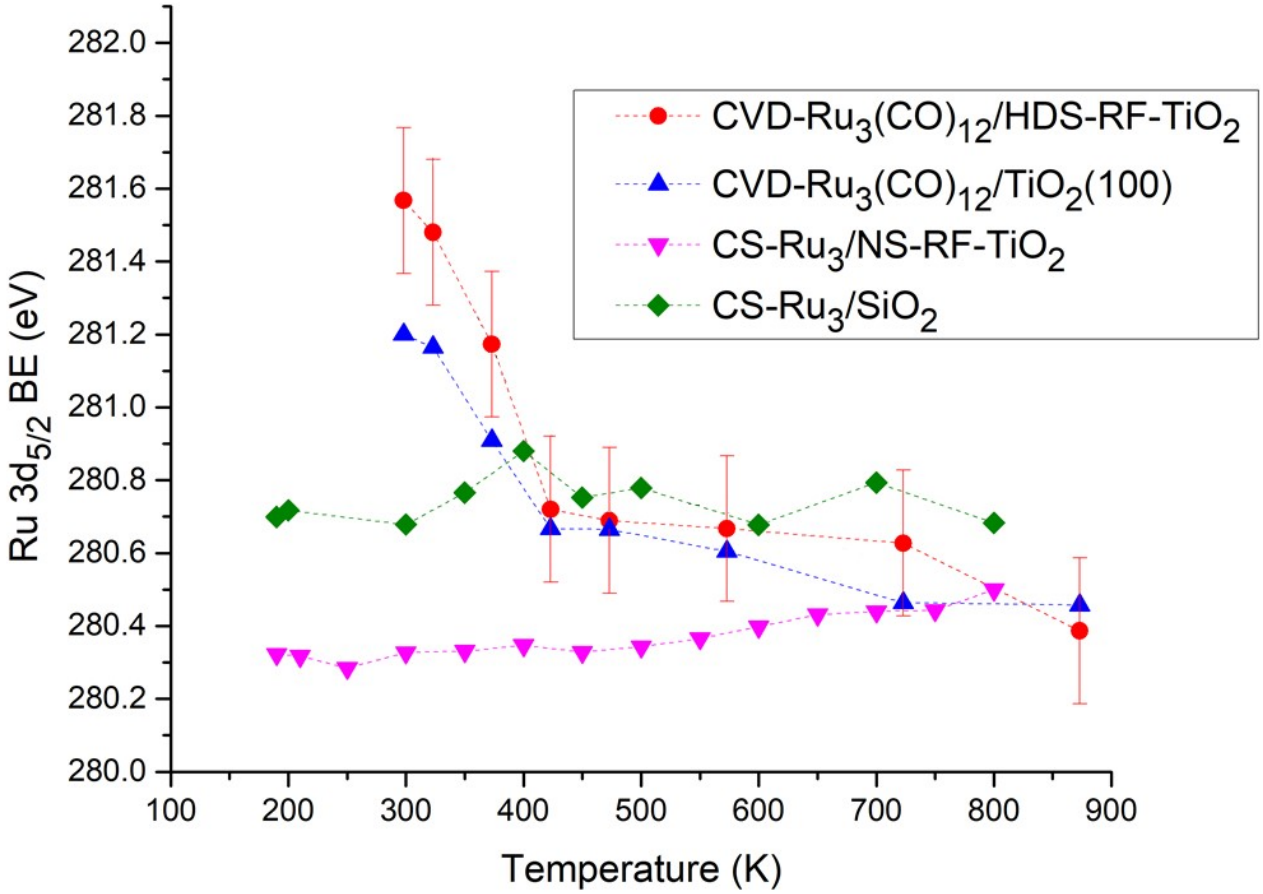

Figure S7: TD-XPS results for Ru $3d_{5/2}$ BE. When fitting $Ru_3(CO)_{12}$ at 373 K this is considered as a transition temperature where two doublets are needed, and the average of the two peak locations are shown. Error bars are for comparing between samples and are the same for all samples but are only displayed for one sample for readability.

For the $Ru_3(CO)_{12}$ samples (Figure S7) the BE initially varied from 281.2 to 282.0 eV between the substrates. As the temperature is increased there is a sharp decrease in BE for these samples which became shallower between 423 and 473 K. It will be shown based on Figure S8 that the change in BE in Figure S7 is due to the removal of the CO ligands. The TD-XPS of CS-Ru_3/NS-RF-TiO_2 showed a slight BE increase with heating which begins at 500 K. The peak shifted further with increased temperature until the total BE shift at 800 K is 0.2 eV ± 0.1 eV. This shift is most likely due to the partial oxidation of Ru clusters by the RF-TiO_2 substrate, which is also suggested in our previous study [14]. The increase in BE at 500 K indicated a temperature of at least 500 K is needed for oxidation to occur. However, the exact stoichiometry of the partially oxidised Ru clusters on the substrates cannot be determined from the XPS results.

CS-Ru_3/SiO_2 (Figure S7) showed no change in Ru BE larger than the uncertainty at any temperature between 190 K and 800 K. This matches our previous results [14] showing that heating to 800 K for temperature programmed desorption (TPD) did not cause a shift in XPS BE. Comparing the two CS samples, the Ru 3d BE is higher for CS-Ru_3/SiO_2 both as-deposited (280.7 eV ± 0.2 eV) and after heat treatment (280.7 eV ± 0.2 eV). This indicated that the cluster-surface interaction between titania and Ru lowered the core Ru 3d BE of the clusters when compared to SiO_2, which is most likely due to the greater extent of charge transfer between the clusters and substrate and/or the formation of a strong metal-substrate interaction (SMSI) with RF-TiO_2 [39].

Figure S8 displays the TD-XPS results for CO/Ru atomic ratios for each ligated $Ru_3(CO)_{12}$ sample. This provides a representation of the CO ligands being removed by the heating procedures. The CO/Ru atomic ratio is determined at each temperature by calculating the ratio between the calibrated peak areas for CO 1s ligands and Ru 3d. For CO 1s, a background level of CO contamination is always present on the samples, even without clusters, and the pre-deposition CO area is subtracted in each case to reduce the effects of this. Also shown are room-temperature blank measurements for CO/Ru atomic ratios; a blank measurement was performed for each cluster sample and the CO/Ru atomic ratios are calculated using the same process as the loaded samples and using the Ru At% from the equivalent cluster-loaded sample.

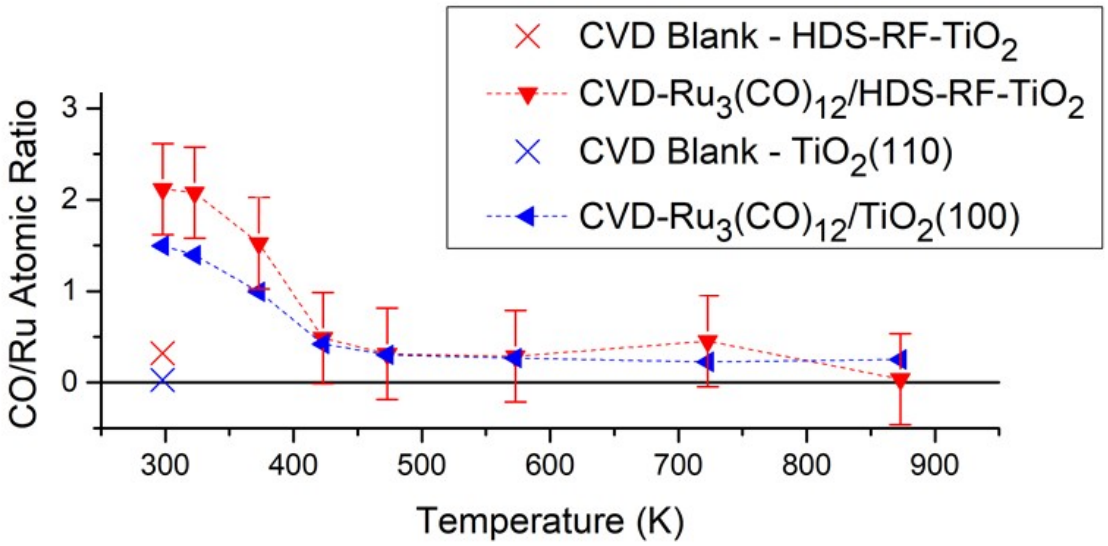

Figure S8: TD-XPS Results - CO/Ru atomic ratios for $Ru_3(CO)_{12}$ depositions. Ratios are determined using XPS At%. Blank, room-temperature measurements are marked using crosses. The fitting uncertainty in CO/Ru atomic ratios is ~13% when comparing between samples, which is reflected in the error bars. The absolute error in the CO/Ru atomic ratio is estimated to be higher at ~0.5. Error bars are the same for all samples but are only displayed for one sample to increase readability.

Figure S8 shows that the blank substrate measurements for the two CVD depositions had little CO adsorbed onto the HDS-RF-TiO_2 or TiO_2(110) substrates after being exposed to CVD conditions with no $Ru_3(CO)_{12}$ present. This indicated that the CO/Ru atomic ratios for the CVD-$Ru_3(CO)_{12}$ samples are not affected significantly by any contamination added during the depositions. The initial CO/Ru atomic ratio is 2.1 ± ~0.5 for CVD-$Ru_3(CO)_{12}$/HDS-RF-TiO_2, and 1.5 ± ~0.5 for CVD-$Ru_3(CO)_{12}$/TiO_2(110). This implies approximate as-deposited chemical formulae of $Ru_3(CO)_6$ and $Ru_3(CO)_{4.5}$ for the clusters in each sample respectively, meaning some ligands are lost in the CVD-procedures. CVD-$Ru_3(CO)_{12}$/HDS-RF-TiO_2 also had a higher Ru 3d BE than CVD-$Ru_3(CO)_{12}$/TiO_2(110), which supports the interpretation that more ligands are lost on TiO_2(110). This aligns with previous measurements by Zhao *et al*. [37], where it is found ligands are desorbed when depositing $Ru_3(CO)_{12}$ onto TiO_2(110) by CVD at room temperature, however in that study the average atomic ratio is determined to be $Ru_3(CO)_{10}$. There thus may be some mechanism for the removal of ligands by TiO_2 at room temperature.

The trends in CO/Ru atomic ratio for the $Ru_3(CO)_{12}$ samples in Figure S8 are similar to one another, and also similar in shape to the trend in Ru $3d_{5/2}$ BE for the same samples in Figure S7. There is a sharp decrease upon heating as the ligands began to desorb, and then the

slope decreased. It appears that for the CVD depositions the trend flattens between 423 K and 473 K, which matched the temperature where the BE trend flattened. The similarity of the trends between the CO/Ru atomic ratio TD-XPS and Ru 3d BE TD-XPS provides support for the interpretation that the initial large decrease in BE with heating for ligated samples is due to the loss of CO ligands. By approximately 423 K most CO ligands had desorbed regardless of the type of TiO_2 substrate or deposition method. For the CVD depositions, at 423 K and above the CO/Ru flatlined to an average of ~0.27. This suggests most of the ligands had been removed, however it is difficult to confirm the complete deligation within the uncertainty (see error bars). The value of ~0.27 may be related to the last ~1 or few ligands. This is supported by the literature where complete deligation has been reported for $Ru_3(CO)_{12}$ on different forms of TiO_2 at between 700 K and 800 K depending on the nature of the substrate and deposition method [37,38], implying 423 K is not a high enough temperature to remove all CO ligands.

The TD-XPS results for Ti^{Defect}/Ti^{Total} atomic ratio for each sample are shown in Figure S9. This figure provides chemical information about the substrate, where the Ti^{Defect}/Ti^{Total} atomic ratio is used as a proxy measurement for the amount of Ti^{3+} and Ti^{2+} surface defects in the substrate. Blank measurements for substrates without deposited clusters were also performed and are displayed on the same axes. These results only applied to the TiO_2 substrates, and the CS-Ru_3/SiO_2 data are not included.

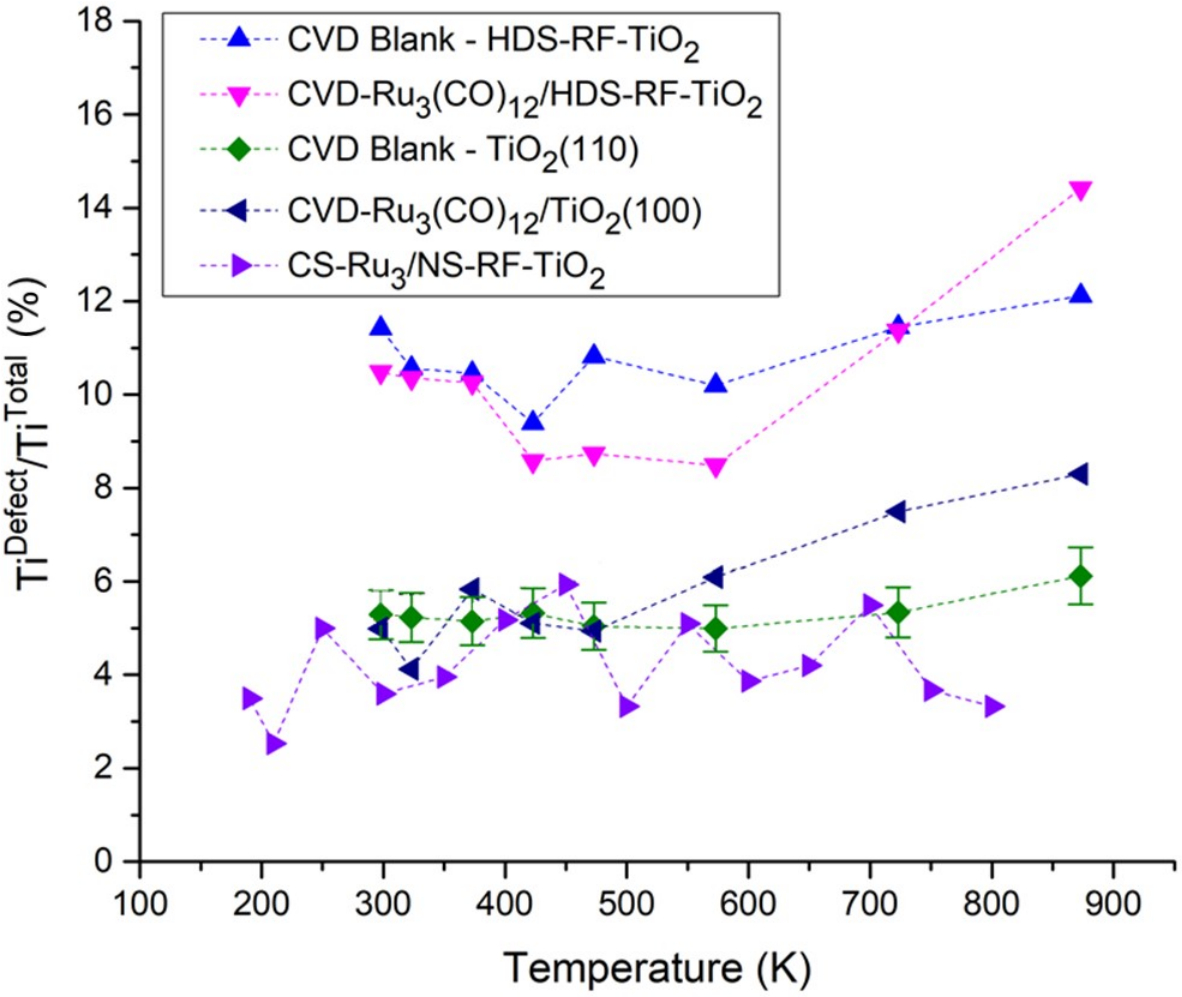

Figure S9: TD-XPS Results - Ti^{Defect}/Ti^{Total} percentage. Percentages are determined from atomic ratios calculated using XPS At%. Blank measurements where no clusters are deposited are included for the CVD depositions. The uncertainty in the fitting of Ti defect ratios is ± 10%, which is shown in the error bars. Error bars are the same for all samples but are only displayed for one to increase readability.

Figure S9 shows that blank HDS-RF-TiO_2 and blank TiO_2(110) for CVD depositions featured small increases in surface defects due to heating, starting at 600 K. However, all $Ru_3(CO)_{12}$-loaded samples increased in Ti defects to a greater extent, beyond the level of blank samples. For CVD-$Ru_3(CO)_{12}$ this started at 573 K on HDS-RF-TiO_2 and at 473 K on TiO_2(110). The difference in Ti defect ratio between the loaded and blank samples after heat treatment is larger than the error bars for CVD-$Ru_3(CO)_{12}$/TiO_2(110), but for CVD-$Ru_3(CO)_{12}$/HDS-RF-TiO_2 the defects increased beyond the blank but there is some overlap in error bars (not shown in Figure S9). Because there is still an increase, and the difference is above the error bars for the other CVD-$Ru_3(CO)_{12}$ sample, it is assumed that the increase

above the blank sample is significant for CVD-$Ru_3(CO)_{12}$/HDS-RF-TiO_2 even with the presence of overlapping error bars.

ARXPS

XPS Fitting Examples

In Figure S10 three spectra are shown with peak fitting for the Ru 3d/C 1s region. These are given as examples and represent the peak fitting procedures used for all ARXPS measurements.

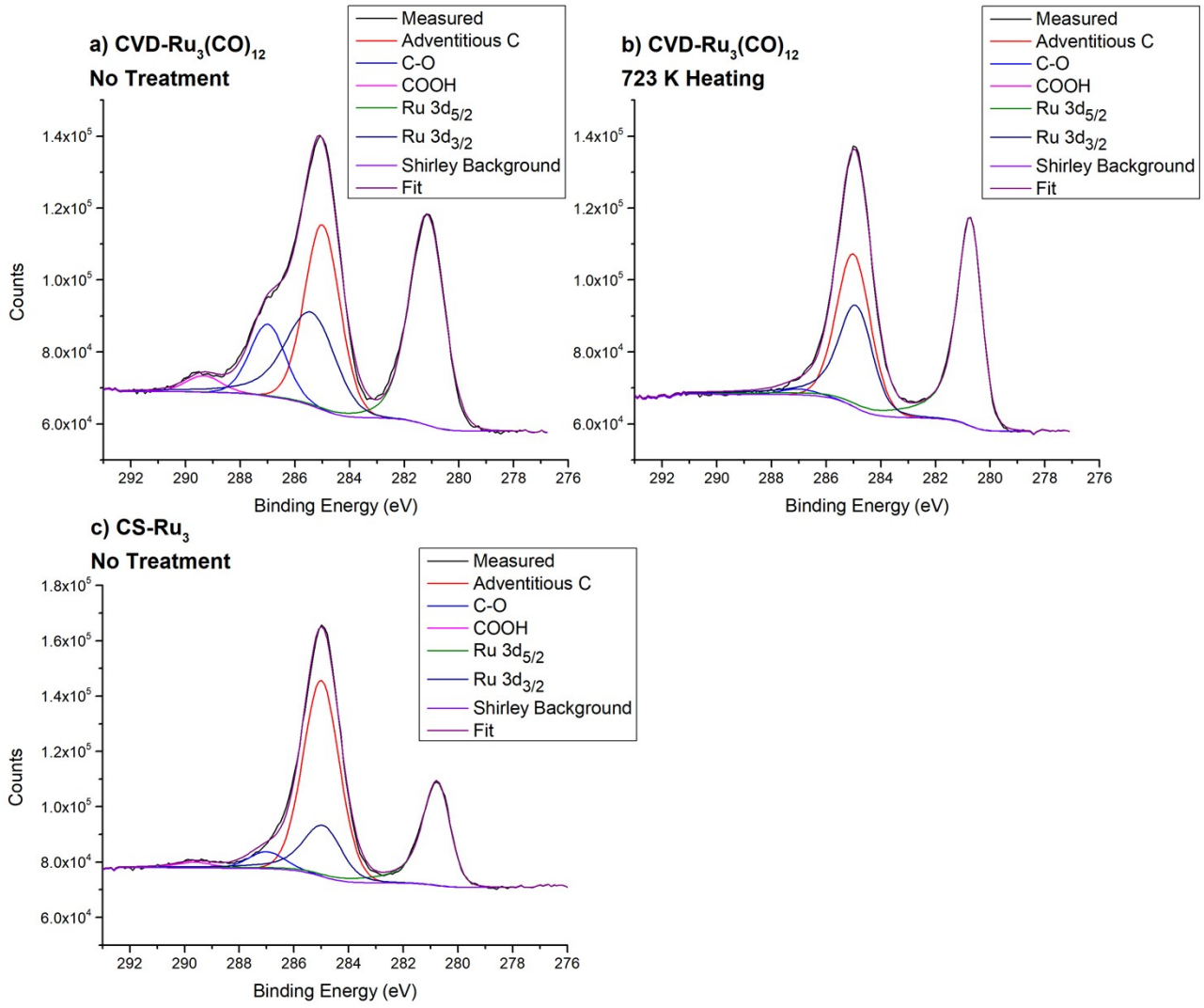

Figure S10: Example peak fitting of the Ru 3d/C 1s region. Measurements are at an observation angle of 0°. a) CVD-$Ru_3(CO)_{12}$/HDS-RF-TiO_2, no treatment. b) CVD-$Ru_3(CO)_{12}$/HDS-RF-TiO_2, 723 K heating. c) CS-Ru_3/HDS-RF-TiO_2, no treatment.

Synchrotron Beam Effects on $Ru_3(CO)_{12}$

Preliminary measurements were performed to determine the effect of the synchrotron X-ray beam on the Ru clusters. It is found that the 720 eV synchrotron X-ray beam is causing the desorption of CO ligands from CVD-$Ru_3(CO)_{12}$. To investigate this, the same cluster spot is

scanned repeatedly at room temperature in series to determine the change in the Ru 3d/C 1s region as the total beam dosed increased. This is performed on a ARXPS CVD-$Ru_3(CO)_{12}$/HDS-RF-TiO_2 sample. The Ru $3d_{5/2}$ BE and CO/Ru atomic ratio are both plotted against the total X-ray beam flux, shown in Figure S11.

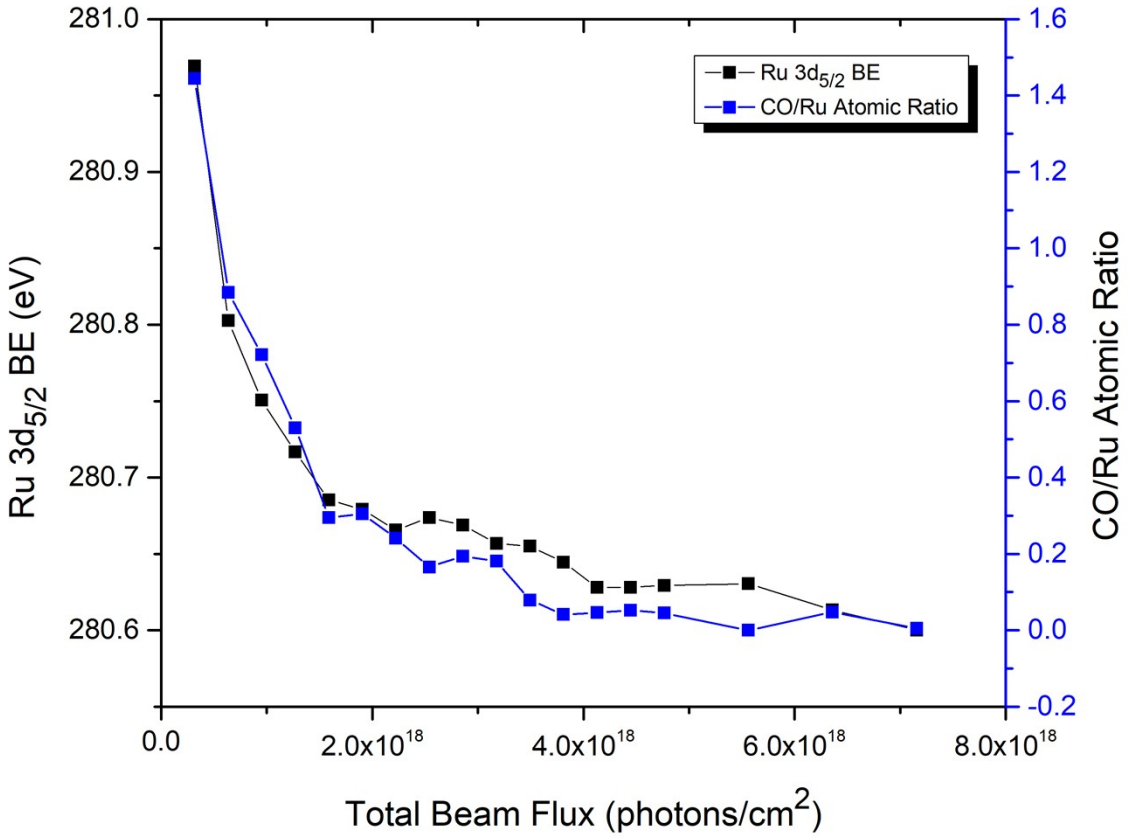

Figure S11: Synchrotron XPS beam effects on CVD-$Ru_3(CO)_{12}$/HDS-RF-TiO_2. The left and right vertical axes show the Ru $3d_{5/2}$ BE and CO/Ru atomic ratio, respectively.

The Ru 3d peak shifted towards lower BE and the CO/Ru atomic ratio decreased as the beam dose increased. Both findings give evidence that the X-ray beam is stripping the CO ligands from the clusters over time. The initial Ru $3d_{5/2}$ BE of 281.0 ± 0.05 eV decreased by 0.4 eV to 280.6 eV ± 0.05 eV after a dose of 7.2 x 10^{18} photons/cm^2. For the TD-XPS measurement in Figure S7, the final BE after heating to 873 K is the same, at 280.6 eV ± 0.2 eV. This indicated that the resulting chemical state is similar whether ligands are removed due to the X-ray beam or heat treatment. Due to these findings, the CVD-$Ru_3(CO)_{12}$/HDS-RF-TiO_2 sample is moved in the X-ray beam spot to a fresh, non-overlapping sample area for each ARXPS scan. It must be mentioned that the CO ligand removal described in this section is not observed when performing laboratory-based XPS measurements (*e.g.* for TD-XPS). This is presumably because synchrotron radiation is typically 10^5-10^{12} times more intense than laboratory X-ray sources [40].

Errors in ARXPS Model

Figure S12 shows the ratios of the difference between experimental and calculated results plotted for each observation angle and temperature. These ratios represent the error between the measured At% and the value in the fitted ARXPS model, on a scale from 0 to 1. The ratios varied per measurement between a ratio of 0 and 0.3. The maximum ratio of 0.3 implied there may have been differences between the modelled depth profile and the true depth profile of the sample. The ratios are consistently higher for particular observation angles regardless of temperature; this may imply that the roughness of the sputtered RF-TiO_2 is an issue for the ARXPS, or that the samples are non-monotonic. Thus, the depth profiles alone are not considered as true quantitative representations of the Ru surface concentration per layer. However, ARXPS can be still used for qualitative indications of changes in depth profile.

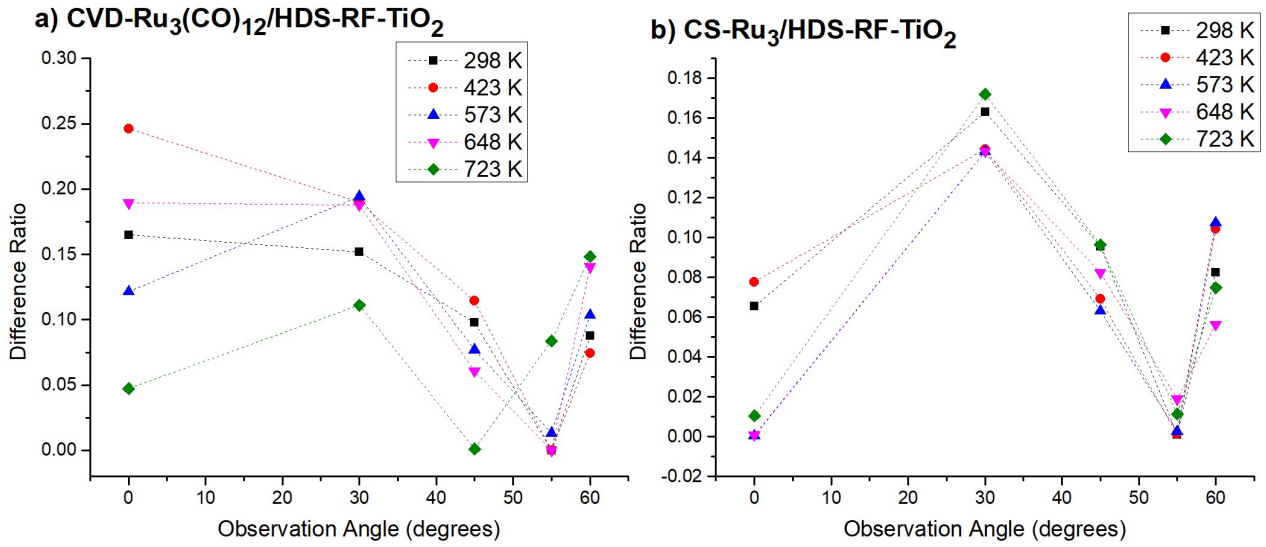

Figure S12: Ratio of the difference between experimental and calculated results at each observation angle and temperature. a) CVD-$Ru_3(CO)_{12}$/HDS-RF-TiO_2. b) CS-Ru_3/HDS-RF-TiO_2.

LEIS

LEIS of Blank Reference Materials

A blank RF-TiO_2 substrate and metallic Ru reference sample were measured with LEIS and the results are shown in Figure S13. From these reference measurements, it is found that the LEIS surface peak locations for the key elements of interest are E/E_0 = 0.85 for Ru, 0.73 for Ti, and 0.41 for O. These measurements are performed at Flinders University, but peak positions are the same on the University of Utah instrument.

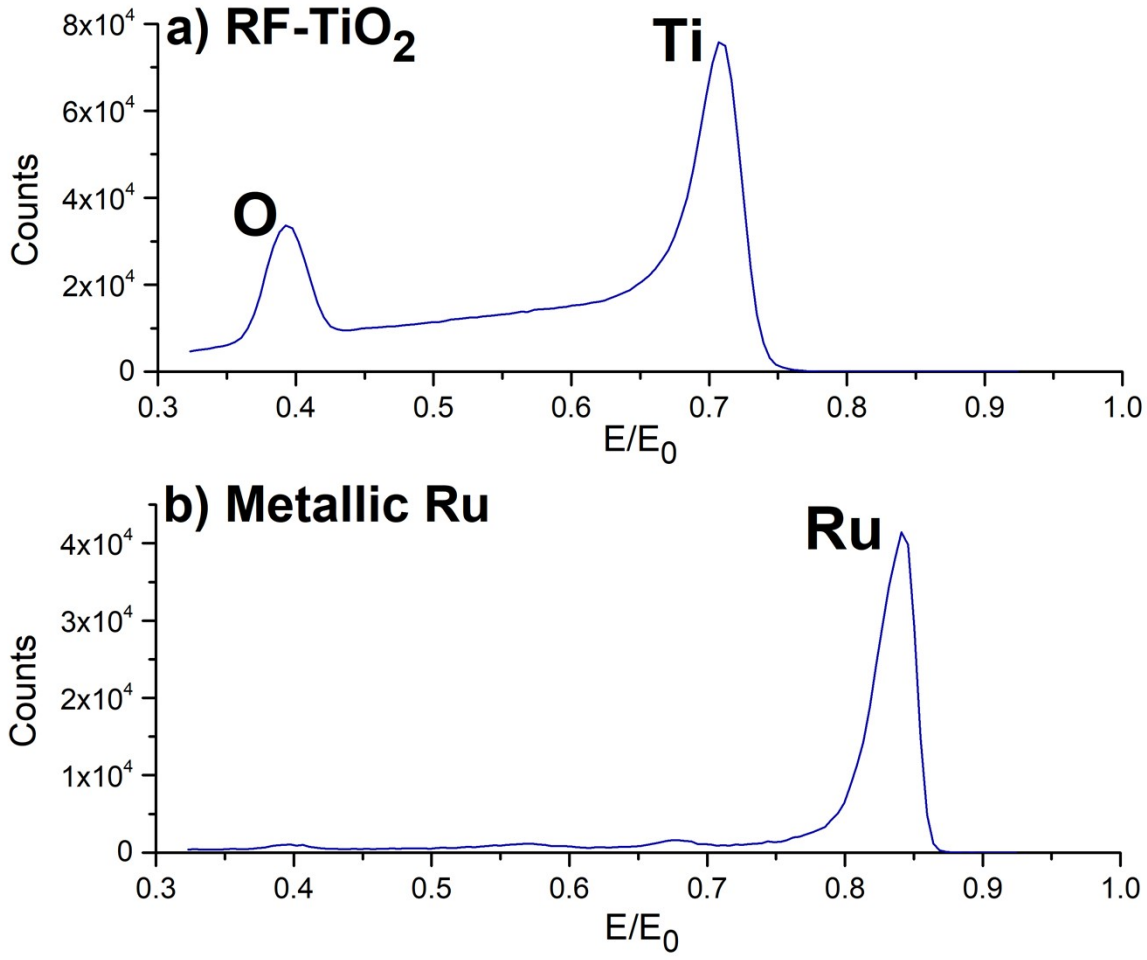

Figure S13: Reference LEIS measurements. a) RF-TiO_2, after heating to 723 K. b) Metallic Ru, after heating to 1073 K and sputter cleaning with 3 keV Ar^+. Some contaminants are present in low concentrations in the metallic Ru, which are visible as 3 smaller peaks at higher E/E_0.

Determination of Ru Removal Rate

To determine the removal rate of Ru by the He^+ beam a LEIS measurement is performed on 800 K heat-treated CS-Ru_3/SiO_2 at The University of Utah. This is the same sample used for TD-LEIS (in main text) and was performed after the main TD-LEIS to not affect the results. Repeated LEIS measurements were performed on a single cluster spot to determine how the ion dose affected the sample. The measured LEIS spectra (not shown) are comparable in features and shape to the CS-Ru_3/SiO_2 LEIS shown in the TD-LEIS measurement in Figure 2a (main text). Figure S14a shows the integrated ratios of Ru/(Si+O) vs. He^+ ion dose. There is no noticeable decrease until ~1 x 10^{15} ions/cm^2, after which the Ru peak size began to decrease. The lack of initial change in peak size is likely due to the presence of some carbonaceous contamination atop the Ru clusters which is sputtered off by the He^+ beam to expose the Ru.

Figure S14b shows the same LEIS measurement as Figure S14a, but the data is truncated to >1 x 10^{15} ions/cm^2, and the integrated Ru peak area ratio is calibrated to determine the number of Ru atoms per area (based on the fact that 1.5 x 10^{14} Ru atoms/cm^2 are deposited). However, this measurement is performed after the main TD-LEIS measurement (shown in Figure 2a, main text), and the TD-LEIS showed that after heating to 800 K, the Ru peak area ratio and therefore number of surface atoms had decreased to 0.43 times the initial value due to agglomeration. This meant that 0.43 times the initial, as-deposited surface concentration is present for the removal rate measurement. The integrated peak area ratio is calibrated linearly based on this known starting value to determine the surface concentration at each ion dose. In LEIS there may be changes in the surface peak due to structural changes as well as concentration changes [24,41], but for the purpose of cluster removal estimation this is neglected and it is reasonably assumed that the cluster structure did not drastically change due to LEIS.

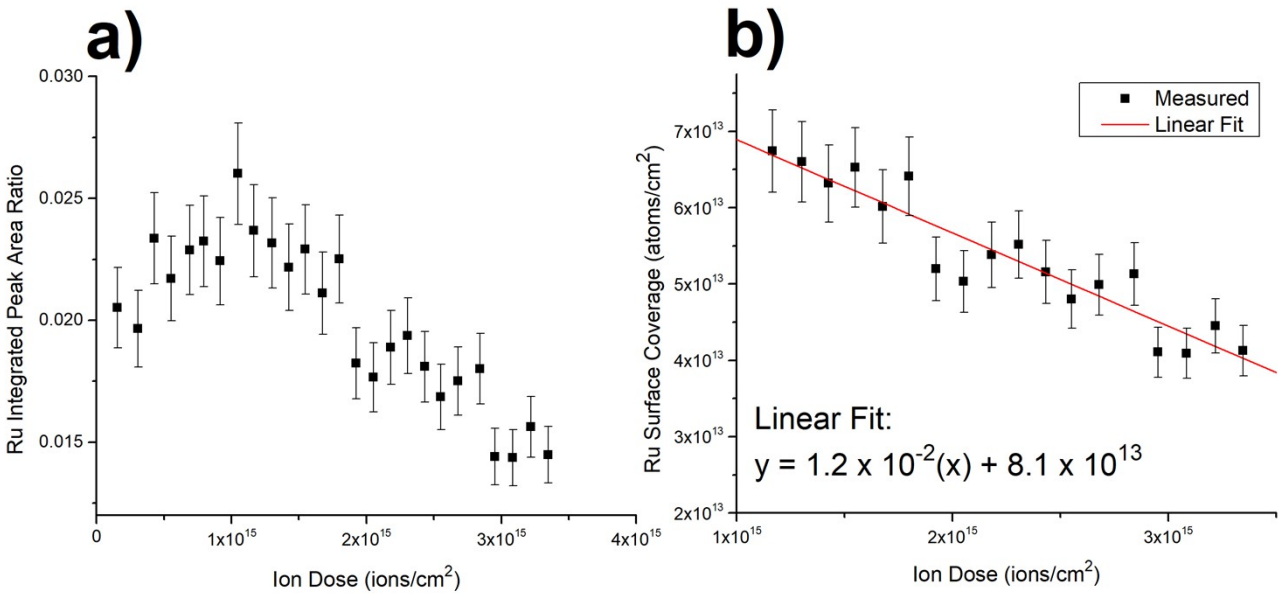

Figure S14: Series LEIS measurement of CS-Ru_3/SiO_2 after heating to 800 K. a) Ru integrated peak ratios vs. cumulative ion dose. b) Calibrated graph of Ru surface coverage vs. cumulative ion dose. (b) is truncated to data points > 1 x 10^{15} ions/cm^2 (discussed in text), and a linear fitting is produced and shown in the figure inset. Uncertainties in Ru peak ratios are ~8%.

The linear fitting for Ru surface coverage vs. ion dose produced in Figure S14b had a slope of -1.2 x 10^{-2} atoms/ion, and an offset of 8.1 x 10^{13} atoms/cm^2. The offset is related to the initial surface concentration of Ru atoms. The negative slope gave the removal rate for Ru atoms by 1 keV He^+, where an average of 1.2 x 10^{-2} Ru atoms are removed by each He^+ projectile. This removal rate is used in calculations of the surface Ru cluster removal for each TD-LEIS measurement.

Ru Surface Coverage and Ion Dosage

XPS was performed on each of the TD-LEIS samples after the TD-LEIS measurements were completed to estimate Ru surface coverage and check for damage induced during the LEIS measurements. These XPS results are given in Table S4. The ratio of total carbon atoms to Ru atoms is calculated and provides a measure of the level of contamination on each sample. In addition, the total ion dose for each measurement is shown, along with the estimated percentage of Ru removed by the He^+ which is used as a measurement for the level of Ru cluster removal due to LEIS. Between all TD-LEIS samples, the percentage of Ru sputtered from the surface during a measurement is an average of 2.9%, and a maximum of 6.8%. These values are cumulative over the TD-LEIS measurements at all temperatures, and this level of cluster removal is small enough that He^+ beam effects can be neglected as a justification for any changes to Ru peaks in TD-LEIS spectra.

Table S4: Ru At%, Ru surface coverage, C/Ru ratio, total He^+ dose, and total removed Ru for all TD-LEIS samples. Measurements are after TD-LEIS, and the samples are heated to 900 K.

Deposition	Substrate	Ru At% (%)	Ru Surface Coverage (% ML)	C/Ru Atomic Ratio	Total Ion Dose (ions/cm^2)	Total Ru Removed (%)
CS-Ru_3	SiO_2	0.5	3	5.4	1.2 x 10^{15}	1.3
CVD-$Ru_3(CO)_{12}$	HDS-RF-TiO_2	1.5	11	1.5	6.0 x 10^{15}	6.8
CS-Ru_3	NS-RF-TiO_2	0.4	3	12.4	1.8 x 10^{15}	2.1
CS-Ru_3	LDS-RF-TiO_2	0.3	2	13.9	1.9 x 10^{15}	2.1
CS-Ru_3	HDS-RF-TiO_2	0.3	2	8.4	1.8 x 10^{15}	2.0

CVD-$Ru_3(CO)_{12}$/HDS-RF-TiO_2 Overlayer Thickness

To determine the thickness of the overlayer, ΔE is divided by the stopping power of titania to give the total length of titania which the He^+ projectiles travelled through, L. The beam impact angle (45°) and the angle to the detector (90°) are incorporated using a scaling factor based on right-angle trigonometry to determine the titania depth D. This relationship is shown in Equation S1.

$$D = 0.414\,L = \frac{0.414\,\Delta E}{Stopping\ Power} \qquad \text{S1}$$

The software package Stopping and Range of Ions in Matter (SRIM) is used to calculate the

stopping power of He^+ ions in TiO_2; 30 ± 3 eV/nm (see supplementary information, page 10 for further details). This calculation uses Bragg's rule [34], and thus any effect of the specific structure of RF-TiO_2 on the stopping power is neglected. Based on Equation S1, it is determined that the average D = 0.35 nm ± 0.08 nm, which is approximately 1.7 ML of titania.

TD-LEIS of CS-Ru_3/RF-TiO_2

TD-LEIS was performed on CS-Ru_3 with 3 different substrate preparation methods: NS-, LDS-, and HDS-RF-TiO_2. These were 3 unique depositions onto different substrates. XPS is performed on each of the TD-LEIS samples after the TD-LEIS measurements were completed, to estimate Ru surface coverage. The XPS result are shown in Table S4, and the TD-LEIS results are shown in Figure S15. The Ru peak is not clearly visible in the LEIS spectra, which is discussed below.

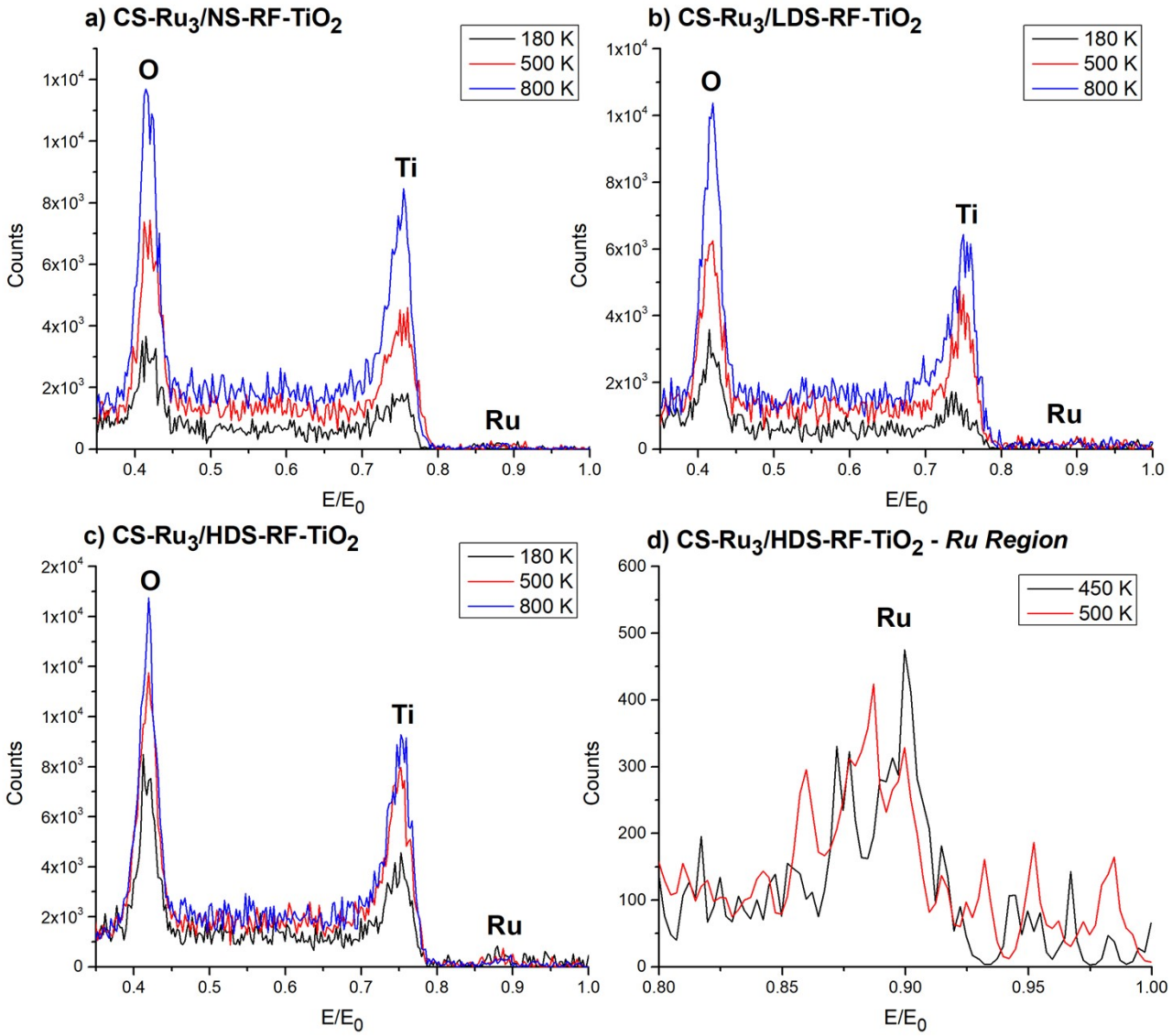

Figure S15: TD-LEIS of CS-Ru_3 on NS-, LDS-, and HDS-RF-TiO_2. Scanned at 14 temperatures between 180 K and 800 K. Selected temperature spectra are shown. a) CS-Ru_3/NS-RF-TiO_2. b) CS-Ru_3/LDS-RF-TiO_2. c) CS-Ru_3/HDS-RF-TiO_2. d) 450 K and 500 K spectra for CS-Ru_3/HDS-RF-TiO_2, zoomed in to the Ru peak region.

In each of Figure S15a-c the total count rate increased after heating which is indicative of surface contaminants being removed. Figure S15a and Figure S15b both showed no clear Ru peak. The measurement in Figure S15a is repeated with a separate sample to check the reliability, and the results are identical (not shown). Figure S15c featured a small Ru peak at intermediate temperatures, from 400 K to 700 K. These peaks are smaller than expected, for example, when compared to the TD-LEIS of CS-Ru_3/SiO_2 in Figure 2a (main text). The fact that CS-Ru_3 peaks are generally not visible in LEIS on the RF-TiO_2 substrates is different to the behaviour of CVD-$Ru_3(CO)_{12}$/HDS-RF-TiO_2 (see Figure 3a, main text), where the clusters are covered by the substrate, but the Ru peak is still visible in the LEIS spectrum at reduced E/E_0. Because an Ru peak is still visible for CVD-$Ru_3(CO)_{12}$/HDS-RF-TiO_2 after encapsulation, the mechanism for the lack of visible peaks for CS-Ru_3 is likely different.

In Table S4, the C/Ru atomic ratio is 12.4, 13.9, and 8.4 for the NS-, LDS-, and HDS-RF-TiO_2, respectively. CS-Ru_3/HDS-RF-TiO_2 had the lowest C/Ru ratio, and the most visible Ru peaks of the CS-Ru_3/RF-TiO_2 samples (from 400 K to 700 K). Additionally, Ru is most easily visible in the LEIS for CS-Ru_3/SiO_2, where the same amount of Ru is deposited, and the C/Ru ratio is 5.4 (Table S4). Because the CS-Ru_3 samples with lower C/Ru ratios had larger peaks, this opens the possibility of an interpretation that the Ru cluster peaks are being affected by carbonaceous contamination on the surface. To support this interpretation, two additional series LEIS measurements were performed to determine the effects of the He^+ ion dose on the resulting spectra. This is performed for two separate CS-Ru_3/NS-RF-TiO_2 samples: as-deposited, and after heating to 800 K. The results for these measurements are shown in Figure S16.

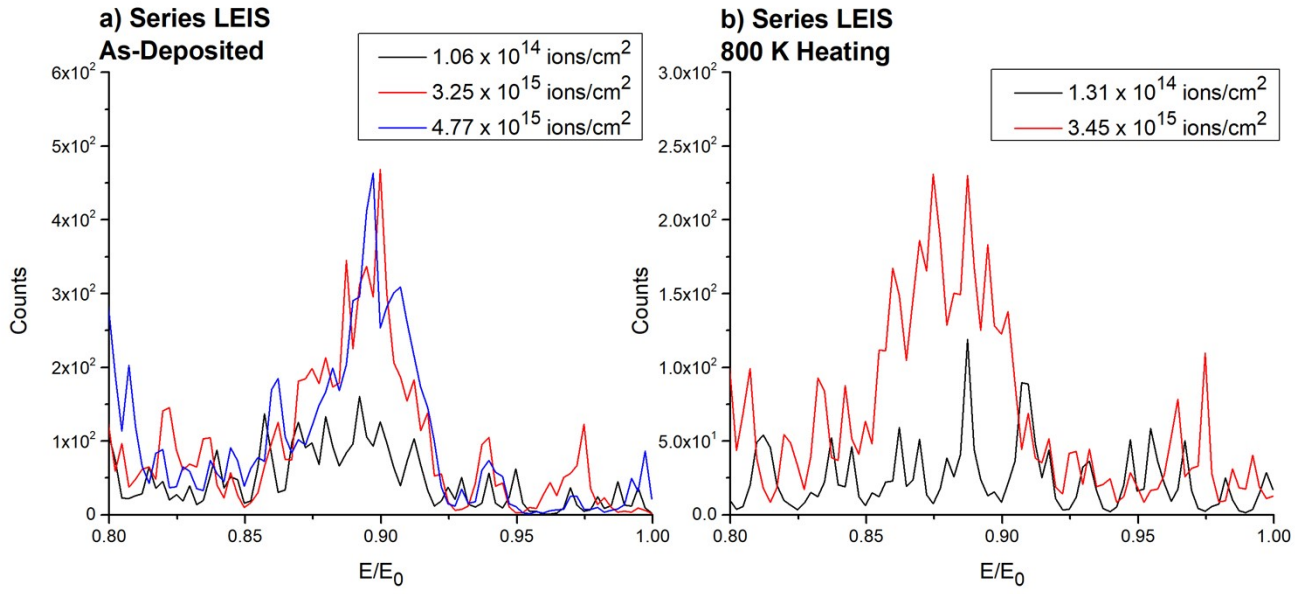

Figure S16: Series LEIS measurements, zoomed into the Ru peak region. a) CS-Ru_3/NS-RF-TiO_2, as-deposited. b) CS-Ru_3/NS-RF-TiO_2, after heating to 800 K. Cumulative doses for the presented scans are given in the legends. Separate samples are used in (a) and (b).

In Figure S16a the Ru region had no peak in the earlier measurements (see the lowest dose scan), but after a dose of 3.25 x 10^{15} ions/cm^2 a small Ru peak is apparent. The Ru peak size did not increase significantly after further sputtering. This indicated that the LEIS He^+ beam had sputtered off a covering layer which is blocking the He^+ from reaching the Ru. In Figure S16b an Ru peak also became visible after a similar dosage of 3.45 x 10^{15} ions/cm^2. Because a small Ru peak is made visible after sputtering the samples with 1 keV He^+, the Ru must have still been close to the surface layer supporting the idea of hydrocarbon-covered clusters. This kind of LEIS signal attenuation by contamination has been seen in previous studies; an example by Brongersma [25] showed that an untreated Au sample

which was exposed to atmosphere featured so much adsorbed hydrocarbons that no Au surface peak is present, even when XPS showed that the sample is high-purity with only minor carbon contamination. There is also the possibility that these clusters interacted with the Ti and/or O on the surface of the substrate in a different way that blocks the availability of the Ru to He^+ projectiles. The TD-LEIS measurements of CS-Ru_3 on RF-TiO_2 could not be repeated with a new RF-TiO_2 substrate featuring less carbon contamination because the collaborative overseas nature of the experiment was time constrained.

STEM of CVD-$Ru_3(CO)_{12}$/HDS-RF-TiO_2

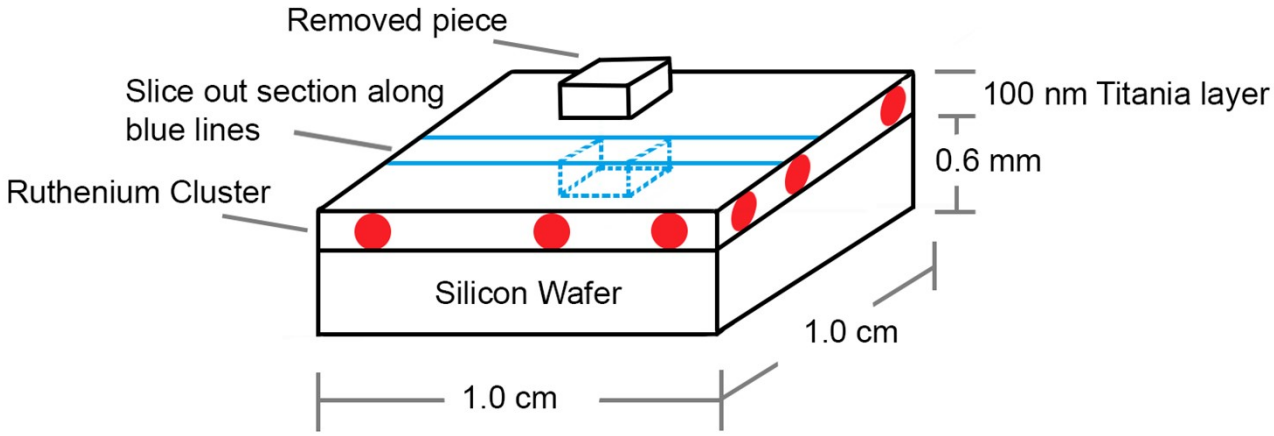

Figure S17: Diagram showing the FIB cutting geometry of the STEM sample. A small piece was removed for analysis, and the dashed blue lines represent the original location of the piece.

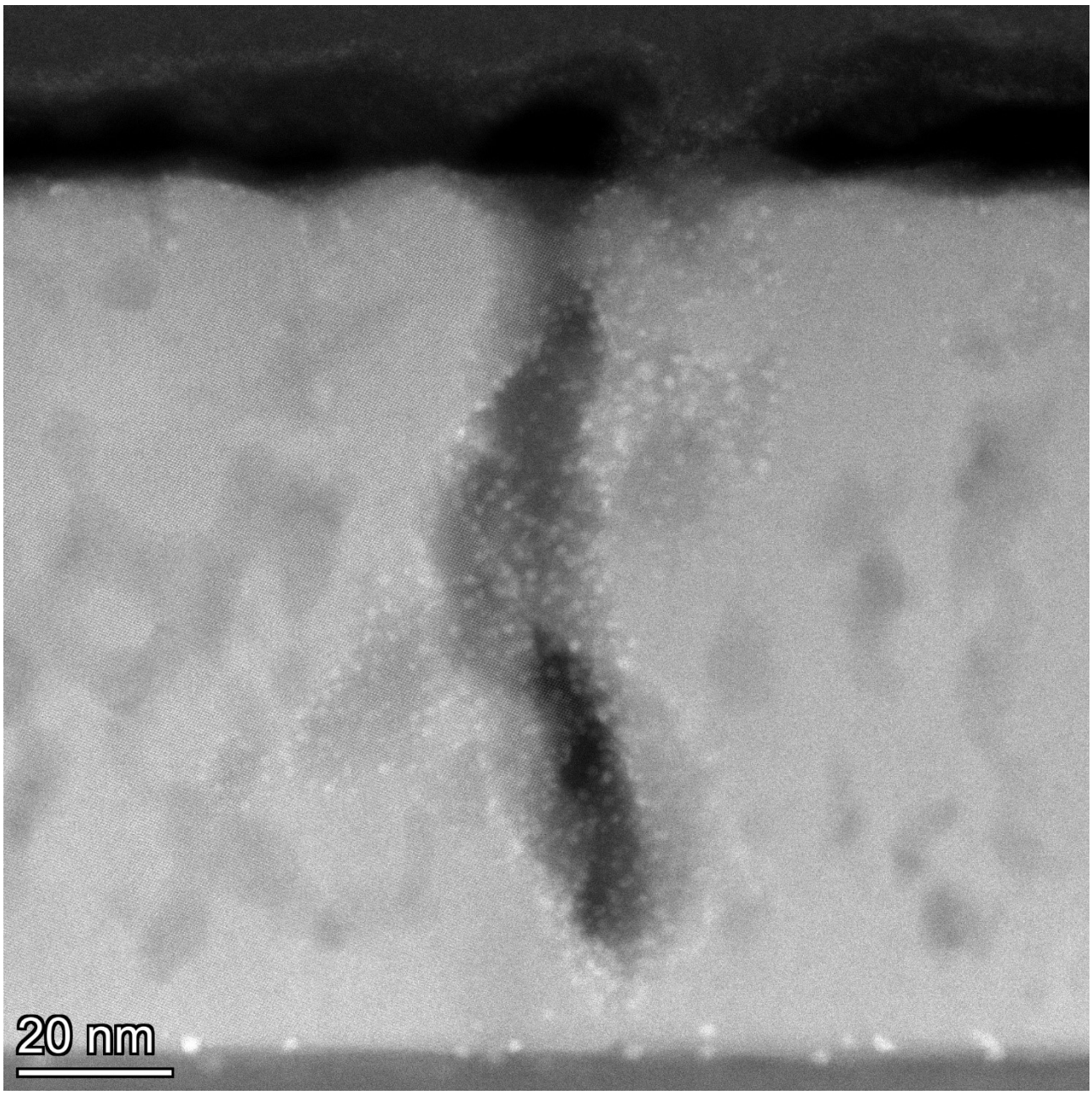

Figure S18: STEM results for analysis of CVD-$Ru_3(CO)_{12}$/HDS- RF-TiO_2 after heat treatment at 723 K. This image shows a pore in the RF-TiO_2 surface which is decorated by Ru clusters.

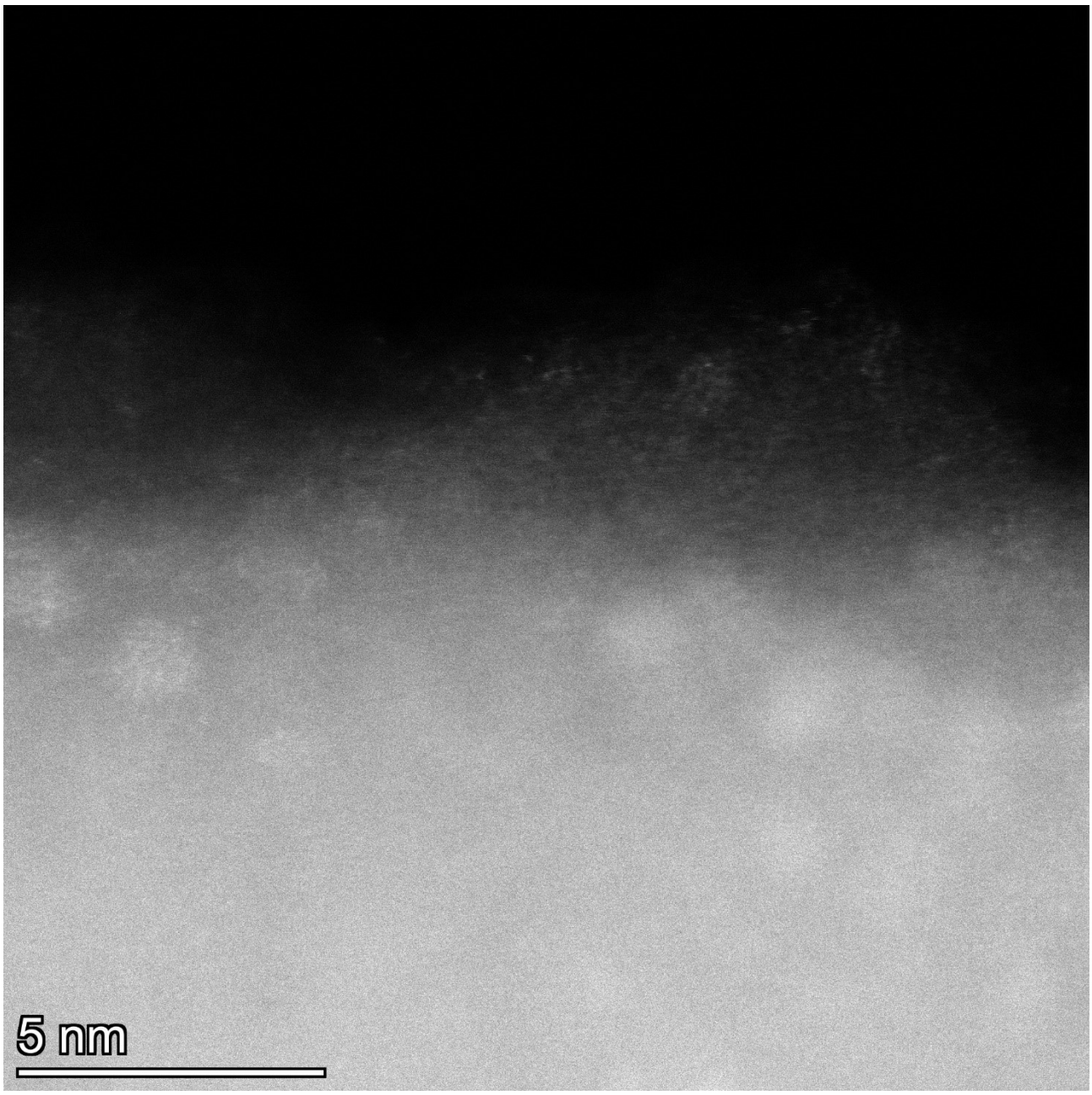

Figure S19: STEM results after heat treatment at 723 K. This image shows a different location on the sample surface to Figure 4a.

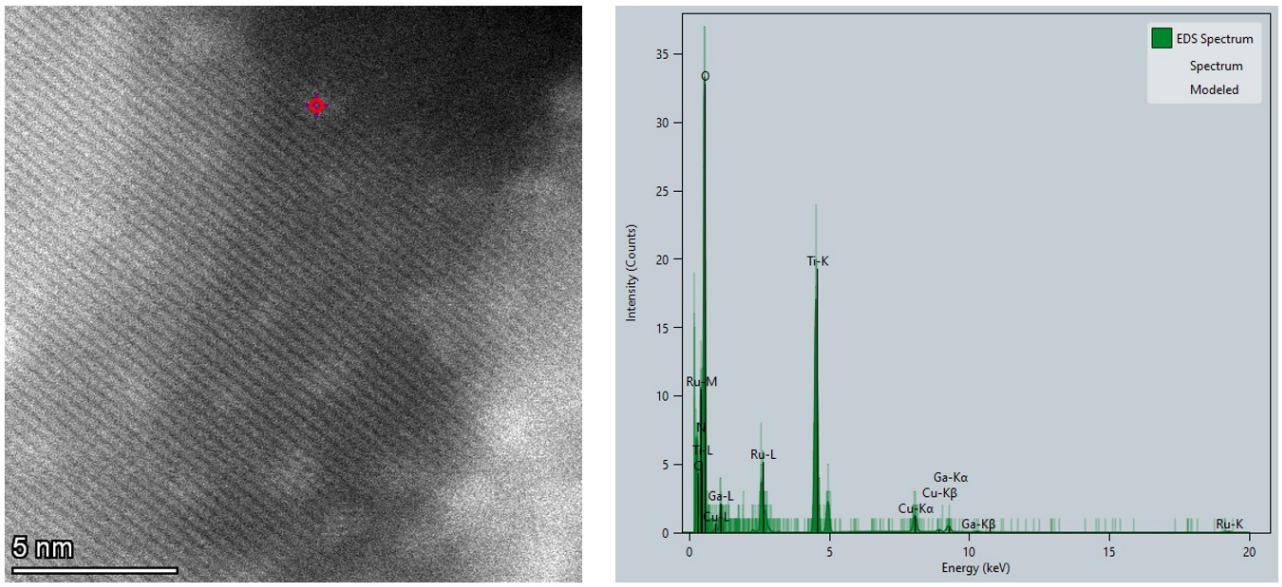

Figure S20: Energy-dispersive X-ray spectrum of a selected cluster location in a STEM image, showing the presence of Ru in the cluster spot.

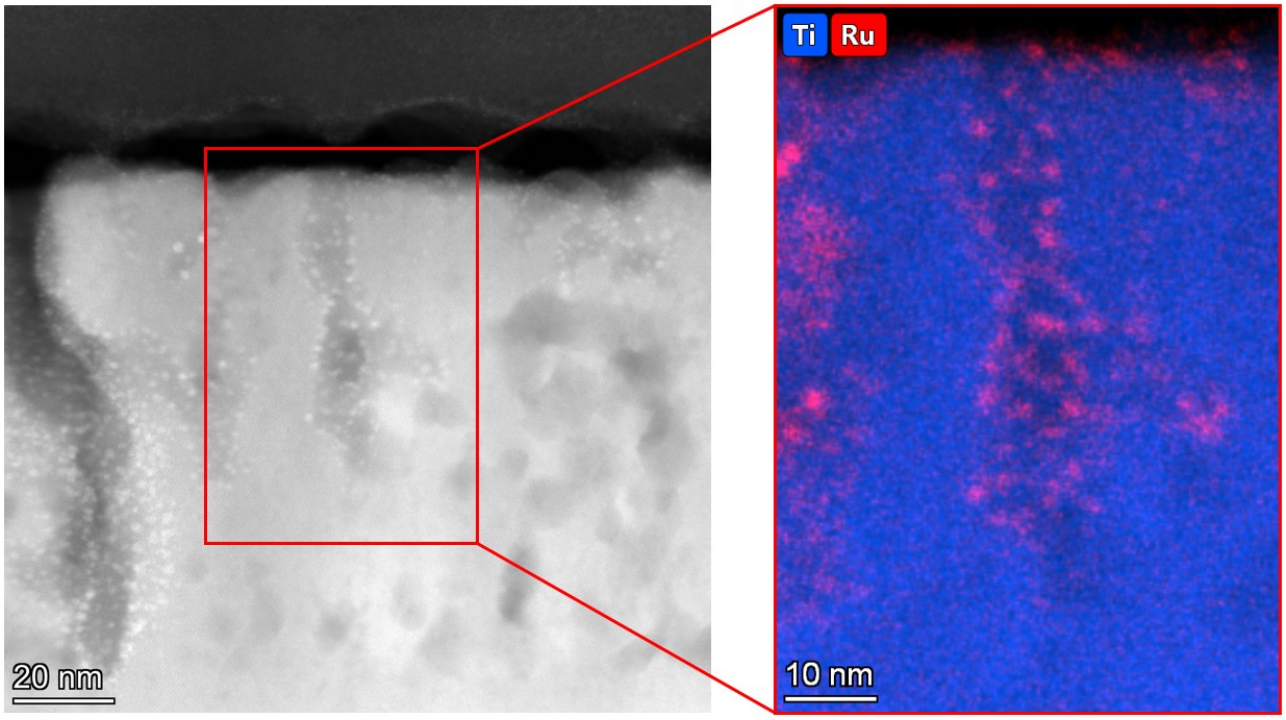

Figure S21: EDX mapping of a pore in the surface ,showing that Ru is present at both the surface and inside the pores.

Table S5: STEM results for cluster diameters, for the numbered clusters from Figure 4a.

Cluster Number	Cluster Diameter (nm)
1	0.9
2	0.9
3	1.4
4	1.6
5	1.1
6	1.3
7	0.9
8	1.0
9	1.1
10	1.2
11	1.1
12	1.0
13	1.3
14	1.4
15	1.3
16	1.4
17	1.5
18	1.3
19	0.9
Mean	**1.2**

References

[1] A. C. Reber, S. N. Khanna, F. S. Roberts, and S. L. Anderson, J. Phys. Chem. C **120**, 2126 (2016).
[2] F. S. Roberts, S. L. Anderson, A. C. Reber, and S. N. Khanna, J. Phys. Chem. C **119**, 6033 (2015).
[3] M. Li, W. Hebenstreit, and U. Diebold, Phys. Rev. B **61**, 4926 (2000).
[4] M. Li, W. Hebenstreit, U. Diebold, A. M. Tyryshkin, M. K. Bowman, G. G. Dunham, and M. A. Henderson, J. Phys. Chem. B **104**, 4944 (2000).
[5] W. E. Kaden, W. A. Kunkel, F. S. Roberts, M. Kane, and S. L. Anderson, J. Chem. Phys. **136**, 204705 (2012).
[6] D. Chandra, M. Garner, and K. Lau, J. Phase. Equilib. **20**, 565 (1999).
[7] H. Haberland, Mall, M., Moseler, M., Qiang, Y., Reiners, T., and Thurner, Y., J. Vac. Sci. Technol. A **12**, 2925 (1994).
[8] H. Haberland, Karrais, M., Mall, M., and Thurner, Y., J. Vac. Sci. Technol. A **10**, 3266 (1992).
[9] V. N. Popok, I. Barke, E. E. B. Campbell, and K.-H. Meiwes-Broer, Surf. Sci. Rep. **66**, 347

(2011).
[10] W. E. Kaden, W. A. Kunkel, and S. L. Anderson, J. Chem. Phys. **131**, 114701 (2009).
[11] M. Aizawa, S. Lee, and S. L. Anderson, Surface Science **542**, 253 (2003).
[12] J. Castle and A. Salvi, J. Electron. Spectrosc. Relat. Phenom. **114**, 1103 (2001).
[13] E. L. Strein and D. Allred, Thin Solid Films **517**, 1011 (2008).
[14] L. Howard-Fabretto, T. J. Gorey, G. Li, S. Tesana, G. F. Metha, S. L. Anderson, and G. G. Andersson, Nanoscale Advances (2021).
[15] D. J. Morgan, Surf. Interface Anal. **47**, 1072 (2015).
[16] Y. J. Kim, Y. Gao, and S. A. Chambers, Appl. Surf. Sci. **120**, 250 (1997).
[17] J. Riga, C. Tenret-Noel, J.-J. Pireaux, R. Caudano, J. Verbist, and Y. Gobillon, Phys. Scr. **16**, 351 (1977).
[18] J. Chastain, *Handbook of X-ray photoelectron spectroscopy* (Perkin-Elmer Corporation, Minnesota, USA, 1992), p. 221.
[19] L. Sutton, *Tables of interatomic distances and configuration in molecules and ions* (Chemical Society, 1965), 11.
[20] G. Fuentes, E. Elizalde, F. Yubero, and J. Sanz, Surf. Interface Anal. **33**, 230 (2002).
[21] G. Bertuccio and D. Maiocchi, J. Appl. Phys. **92**, 1248 (2002).
[22] F. Eschen, M. Heyerhoff, H. Morgner, and J. Vogt, J. Phys. Condens. Matter **7**, 1961 (1995).
[23] C. Wang and G. G. Andersson, Surf. Sci. **605**, 889 (2011).
[24] G. Li, B. Zandkarimi, A. C. Cass, T. J. Gorey, B. J. Allen, A. N. Alexandrova, and S. L. Anderson, J. Chem. Phys. **152**, 024702 (2020).
[25] H. H. Brongersma, Characterization of Materials, 1 (2012).
[26] M. D. Kane, F. S. Roberts, and S. L. Anderson, Int. J. Mass Spectrom. Ion Processes **370**, 1 (2014).
[27] Y. Dai, T. J. Gorey, S. L. Anderson, S. Lee, S. Lee, S. Seifert, and R. E. Winans, J. Phys. Chem. C **121**, 361 (2017).
[28] E. T. Baxter, M.-A. Ha, A. C. Cass, A. N. Alexandrova, and S. L. Anderson, ACS Catal. **7**, 3322 (2017).
[29] E. T. Baxter, M.-A. Ha, A. C. Cass, H. Zhai, A. N. Alexandrova, and S. L. Anderson, J. Phys. Chem. C **122**, 1631 (2018).
[30] T. J. Gorey, B. Zandkarimi, G. Li, E. T. Baxter, A. N. Alexandrova, and S. L. Anderson, J. Phys. Chem. C **123**, 16194 (2019).
[31] T. J. Gorey, Y. Dai, S. L. Anderson, S. Lee, S. Lee, S. Seifert, and R. E. Winans, Surf. Sci. **691**, 121485 (2020).
[32] B. Zandkarimi, T. J. Gorey, G. Li, J. Munarriz, S. L. Anderson, and A. N. Alexandrova, Chem. Mater. **32**, 8595 (2020).
[33] J. F. Ziegler, M. D. Ziegler, and J. P. Biersack, Nucl. Instrum. Methods Phys. Res., B **268**, 1818 (2010).
[34] W. H. Bragg and R. Kleeman, Lond. Edinb. Dubl. Phil. Mag. **10**, 318 (1905).
[35] J. W. Rabalais, *Principles and applications of ion scattering spectrometry: surface chemical and structural analysis* (Wiley New York, 2003), Wiley-Interscience Series on Mass Spectrometry.
[36] J. W. Arblaster, Platinum Met. Rev. **57**, 127 (2013).
[37] X. Zhao, J. Hrbek, and J. A. Rodriguez, Surf. Sci. **575**, 115 (2005).
[38] D. Meier, G. Rizzi, G. Granozzi, X. Lai, and D. Goodman, Langmuir **18**, 698 (2002).
[39] U. Diebold, Surf. Sci. Rep. **48**, 53 (2003).
[40] Z. Gong and Y. Yang, J. Energy Chem. **27**, 1566 (2018).
[41] H. H. Brongersma, M. Draxler, M. De Ridder, and P. Bauer, Surf. Sci. Rep. **62**, 63 (2007).